Biomaterials 294 (2023) 121985

Contents lists available at ScienceDirect

Biomaterials

journal homepage: www.elsevier.com/locate/biomaterials

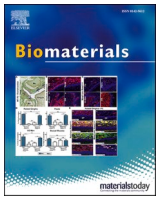

An injectable PEG-like conjugate forms a subcutaneous depot and enables sustained delivery of a peptide drug

Imran Ozer [a,1], Anna Slezak [b,2], Parul Sirohi [a], Xinghai Li [a], Nikita Zakharov [a], Yunxin Yao [b], Jeffrey I. Everitt [c], Ivan Spasojevic [d,e], Stephen L. Craig [b], Joel H. Collier [a], Jonathan E. Campbell [f,g,h], David A. D'Alessio [f,g], Ashutosh Chilkoti [a,*]

[a] Department of Biomedical Engineering, Duke University, Durham, NC, USA
[b] Department of Chemistry, Duke University, Durham, NC, USA
[c] Department of Pathology, Duke University Medical Center, Durham, NC, USA
[d] Duke School of Medicine, Department of Medicine-Oncology, Durham, NC, USA
[e] Duke Cancer Institute, PK/PD Core Laboratory, Durham, NC, USA
[f] Duke Molecular Physiology Institute, Duke University, Durham, NC, USA
[g] Division of Endocrinology, Duke University Medical Center, Durham, NC, USA
[h] Department of Pharmacology and Cancer Biology, Duke University, Durham, NC, USA

ARTICLE INFO

Classification:
Biological sciences
Applied biological sciences
Physical sciences
Peptide drugs
Sustained drug release
Drug depot
PEG

ABSTRACT

Many biologics have a short plasma half-life, and their conjugation to polyethylene glycol (PEG) is commonly used to solve this problem. However, the improvement in the plasma half-life of PEGylated drugs' is at an asymptote because the development of branched PEG has only had a modest impact on pharmacokinetics and pharmacodynamics. Here, we developed an injectable PEG-like conjugate that forms a subcutaneous depot for the sustained delivery of biologics. The PEG-like conjugate consists of poly[oligo(ethylene glycol) methyl ether methacrylate] (POEGMA) conjugated to exendin, a peptide drug used in the clinic to treat type 2 diabetes. The depot-forming exendin-POEGMA conjugate showed greater efficacy than a PEG conjugate of exendin as well as Bydureon, a clinically approved sustained-release formulation of exendin. The injectable depot-forming exendin-POEGMA conjugate did not elicit an immune response against the polymer, so that it remained effective and safe for long-term management of type 2 diabetes upon chronic administration. In contrast, the PEG conjugate induced an anti-PEG immune response, leading to early clearance and loss of efficacy upon repeat dosing. The exendin-POEGMA depot also showed superior long-term efficacy compared to Bydureon. Collectively, these results suggest that an injectable POEGMA conjugate of biologic drugs that forms a drug depot under the skin, providing favorable pharmacokinetic properties and sustained efficacy while remaining non-immunogenic, offers significant advantages over other commonly used drug delivery technologies.

1. Introduction

Most biologics, with the exception of antibodies, have a short plasma half-life due to their rapid renal elimination and in vivo degradation [1,2]. Their short in vivo half-life hence necessitates frequent injections, resulting in a peak-and-valley profile in drug concentration that is pharmacologically suboptimal. It also incurs a high treatment cost and poor patient compliance because of the need for frequent drug administration and the side effects associate with a peak-and-valley drug concentration profile [3,4].

One of the most common approaches to overcome these challenges is the covalent attachment of biologics to polyethylene glycol (PEG), a technology that is colloquially termed PEGylation [5]. Unfortunately, PEGylation has several significant limitations, First, PEGylated therapeutics induce varying titers of PEG antibodies upon treatment [6–8]. Pre-existing PEG antibodies have also been reported in up to 70% of the population who are naïve to PEGylated therapeutics, possibly due to chronic exposure to PEG in consumer products and because PEG is used

* Corresponding author.
E-mail address: chilkoti@duke.edu (A. Chilkoti).
[1] Present address: The Boston Consulting Group, San Francisco Bay Area, CA, USA.
[2] Present address: Pritzker School of Molecular Engineering, University of Chicago, Chicago, IL, USA.

https://doi.org/10.1016/j.biomaterials.2022.121985
Received 1 August 2022; Received in revised form 20 December 2022; Accepted 22 December 2022
Available online 3 January 2023

as an excipient in many drug formulations [9–11]. When present at high titers, both induced and pre-existing PEG antibodies have caused a severe allergic reaction and accelerated clearance in some patients, reducing the drugs' clinical efficacy [7,8,12,13]. These issues have collectively led to the early termination of several clinical trials of PEGylated drug candidates and the withdrawal of several PEGylated therapeutics from the market [12,14,15]. Second, attempts to improve the pharmacokinetics (PK) of PEG have focused on synthesizing branched and star-shaped PEGs. However, these architectures have a modest effect on PK [16] and have antigenic and immunogenic profiles similar to linear PEG [12]. The optimization of PEG is now at an asymptote, and new architectures that radically depart from linear PEG are needed to address these limitations.

Motivated by these needs, we have developed poly[oligo(ethylene glycol) methyl ether methacrylate] (POEGMA) as a next-generation PEG-like polymer for conjugation to biologics. POEGMA is an amphiphilic, hyperbranched polymer that breaks up the long ethylene glycol sequences in PEG and presents them as much shorter oligomeric ethylene glycol (OEG) sidechains along a hydrophobic backbone [17,18]. We previously showed that a soluble POEGMA conjugate eliminates PEG immunogenicity of a PEGylated protein [19] and RNA aptamer drugs [20] while retaining its lack of reactivity towards PEG antibodies. We also previously showed that soluble POEGMA improves the PK of exendin-4, a peptide drug used in the clinic to treat type 2 diabetes (T2D) and subsequently referred to herein as exendin [17]. Although these results were encouraging, the soluble Ex-POEGMA conjugate reported previously only showed a modest improvement in the PK and pharmacodynamics (PD) of the drug, and no comparison to PEG conjugates were made in that study.

We report here a new approach to enhance the PK and PD beyond that afforded by soluble POEGMA and PEG conjugates. This approach consists of a new —next-generation— POEGMA copolymer is conjugated to exendin, and is soluble at room temperature, but undergoes a phase transition at body temperature upon subcutaneous (s.c.) injection to form a coacervate —an insoluble phase— in vivo. This injectable depot formulation of the Ex-POEGMA conjugate exhibits sustained release from the depot into the blood while retaining its lack of immunogenicity. The depot-forming Ex-POEGMA conjugate extended the PK and PD of exendin well beyond that of the first generation soluble POEGMA and size-matched PEG conjugates and had also better efficacy than a clinically used sustained release formulation of exendin.

2. Results

2.1. Injectable and depot forming POEGMA library

It has been previously reported that POEGMA exhibits lower critical solution temperature (LCST) phase behavior, allowing it to transition between an aqueous soluble and insoluble coacervate phase in a temperature- and concentration-dependent manner [21–24]. Here, we exploited this feature to design a soluble conjugate that forms a depot under the skin and provides sustained drug release from the POEGMA depot into circulation. To do so, we first identified POEGMAs that would be suitable as an injectable depot by creating a set of POEGMAs with azide-end groups (Figs. S1–2) by activator-regenerated by electron transfer atom transfer radical polymerization (ARGET-ATRP) [25] that phase transition between room temperature (25 °C) and the subcutaneous (s.c.) temperature of mice (34 °C) [26]. We restricted the EG side-chain length to ≤3 (Figs. S3–6) because previous studies showed that POEGMA conjugates with a side-chain length of >3 had a low, though measurable level of binding to PEG antibodies [17,18]. The phase transition temperature (T_t) of POEGMA was sensitive to the OEG side chain length, with shorter side-chains having a lower T_t due to the decreased hydrogen bonding. The T_t of a homopolymer POEGMA with 3 EG-long side chains (EG3) was too high to form a s.c. depot, while the T_t of an EG2 homopolymer was lower than 25 °C, preventing it from being injected in a soluble form at room temperature.

These observations led us to hypothesize that a random copolymer of POEGMA with EG3 and EG2 units could be synthesized that has a T_t that is between room temperature and body temperature across a range of concentrations relevant for drug delivery, which would be ideal for the design of a conjugate that is injectable, but phase transitions into an insoluble coacervate upon s.c. injection, thereby forming a drug depot. To identify a copolymer with an optimal T_t for an injectable s.c. depot, we synthesized a set of copolymers from EG2 and EG3 monomers, wherein the molar percentage of EG2 ranged from 58 to 100%, as determined by Nuclear Magnetic Resonance (NMR) spectroscopy (Figs. S7–8) [27]. We also synthesized an EG3 POEGMA homopolymer as a non-depot forming —soluble— control. The monomer composition of POEGMA was defined as the percentage of EG2 (or EG3) monomer content in the total polymer. We used the nomenclature of EGX%, where X is the length of the EG chain (2 or 3), and the subscript % is the percentage of the monomer in the total polymer. All synthesized polymers were relatively monodisperse, as measured by gel permeation chromatography-multi-angle light scattering (GPC-MALS), with a polydispersity (Đ) of <1.2 (Fig. 1A; Fig. S9). Their degree of polymerization (DP) ranged from 100 to 400, translating to a weight-averaged molecular weight (M_w) range of 20–80 kDa. Each polymer's monomer composition, M_w, number-averaged molecular weight (M_n), Đ, DP, hydrodynamic size (R_h), and T_t are shown in Figs. S7–10 and are summarized in Table S1.

All polymers showed sharp and thermally reversible phase behavior, as seen by the sharp increase in optical density as the temperature was increased and by the fact that their optical density decreased back to baseline as the temperature was decreased below the T_t (Fig. 1B). Their phase behavior also showed no thermal hysteresis, as seen by the overlapping turbidity curves for the heating and cooling cycle. The $EG3_{100\%}$ POEGMA had a T_t of ~48 °C at 25 μM, consistent with a previous report [24], confirming that it cannot form an s.c. depot. The T_t of the POEGMA copolymers was a function of the EG2 content, as the T_t decreased with increasing molar ratio of the more hydrophobic EG2 monomer. All copolymers phase transitioned between 25 and 34 °C. The T_t of POEGMA also showed an inverse concentration dependence. The T_t increased with POEGMA dilution (Fig. 1C), suggesting that sustained release of a POEGMA conjugate from the s.c. depot should be possible in vivo, in response to continuous dilution at the periphery of the depot. The T_t of POEGMA was also a function of its M_w, as the T_t decreased with increasing DP— and M_w (Fig. 1D). These data showed that all POEGMA copolymers tested were potential depot-forming constructs.

2.2. Identifying an optimal Ex-POEGMA conjugate

We next systematically varied the key molecular variables —the ratio of EG2 to EG3 units and M_w.— to optimize the in vivo phase behavior of the depot-forming POEGMA copolymers. To identify the optimal Ex-POEGMA conjugate that maximizes fed blood glucose control in hyperglycemic mice, we first optimized the T_t, followed by the M_w, and finally the dose of the conjugate. POEGMA copolymers synthesized for the T_t optimization study are shown in Table 1 under the heading –Index: T_t and the copolymers with varied M_w that were synthesized for the M_w optimization study are listed under the heading —Index: M_w.

Conventional conjugation methods typically provide limited control over the conjugation site and stoichiometry, resulting in a heterogeneous mixture of conjugates with non-uniform PK and pharmacodynamics (PD) [28]. To circumvent this issue, we conjugated POEGMA to exendin at its C-terminus using bio-orthogonal click chemistry [17,28–30] We chose the C-terminus as the POEGMA conjugation site, as the N-terminus of exendin was reported to be critical to its function [17]. To do so, we first covalently conjugated a bio-orthogonal triglycine dibenzocyclooctyne (DBCO) group to the C-terminus of exendin via sortase A-mediated native peptide ligation [17,29], yielding

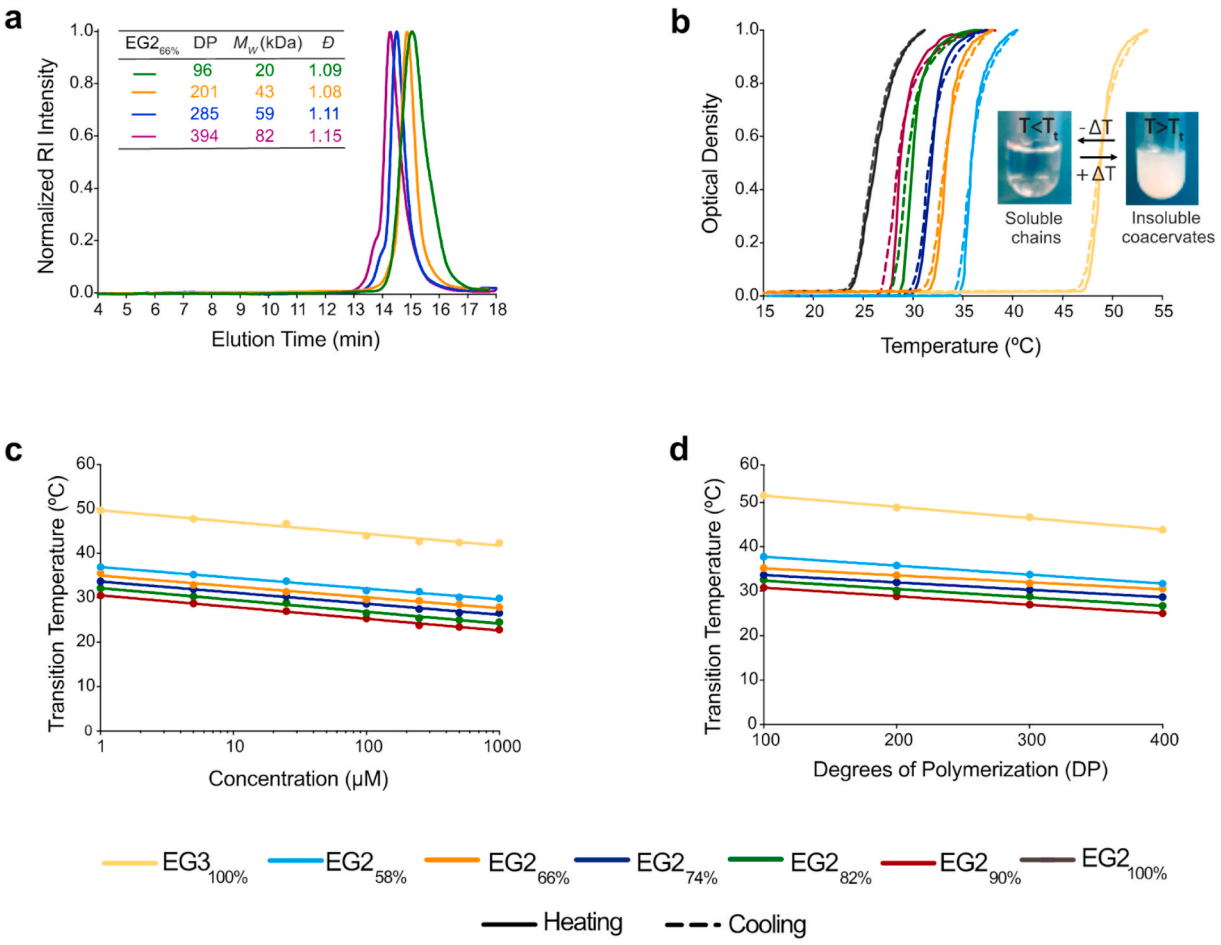

Fig. 1. Well-defined POEGMAs of varying M_w and monomer composition phase-transition near body temperature in a concentration- and M_w-dependent manner and remain soluble at room temperature. (A) GPC chromatogram of $EG2_{66\%}$ copolymers at varied M_w. (B) The optical density of POEGMAs with constant DP but varying monomer composition was monitored as temperature increased (solid line) and decreased (dashed line) to demonstrate the reversibility of phase behavior. Data were shown for POEGMAs at DP 200 and 25 μM. (C) At varying concentrations, the optical density of POEGMAs demonstrates concentration dependence of T_t. Data were shown for POEGMAs at DP 300 in phosphate-buffered saline (PBS). (D) The optical density of POEGMAs with varying DP and monomer composition was monitored to demonstrate T_t's DP dependence. Data were shown for POEGMAs at 25 μM in PBS.

Table 1
Characterization of exendin variants. EG2% was calculated using NMR spectroscopy. M_n, M_w, and Đ values were determined by size exclusion chromatography multi-angle light scattering (SEC-MALS). R_h was measured by dynamic light scattering (DLS) (n = 10). DP was calculated by dividing polymer M_w by the monomer M_w. The EC_{50} of exendin variants was determined from the dose-response curves in Fig. 2c, i, and Fig. 3c (n = 10). Data are reported as mean ± standard error of the mean (SEM). T_t was measured at 500 μM *Calculated from the amino acid sequence. †Default value due to the monodisperse nature of the peptide. The indices in column 1 of the table —T_t, M_w, and polymer type are explained in the text.

Compound	EG2%	DP	T(°C)	M_w (kDa)	Đ(M_w/M_n)	R_h (nm)	EC_{50} (nM)
Exendin	N/A	N/A	N/A	4.2*	1.00†	2.2 ± 0.1	0.04 ± 0.01
Index: T_t							
$Ex\text{-}POEGMA_{31.9°C}$	48.5	247	31.9	57.7	1.15	4.8 ± 0.7	4.7 ± 0.8
$Ex\text{-}POEGMA_{29.9°C}$	60.5	253	29.9	57.6	1.15	4.4 ± 0.9	3 ± 0.7
$Ex\text{-}POEGMA_{28.4°C}$	68.8	254	28.4	56.9	1.13	4.5 ± 0.7	4.5 ± 1.1
Index: M_w							
$Ex\text{-}POEGMA_{18.9kDa}$	100	71	32.3	18.9	1.03	2.6 ± 0.9	1.2 ± 0.4
$Ex\text{-}POEGMA_{54.3kDa}$	62.5	239	29.6	54.3	1.14	4.2 ± 0.5	2.8 ± 0.7
$Ex\text{-}POEGMA_{99.4kDa}$	56.8	454	29	99.4	1.13	4.5 ± 1.1	1.4 ± 0.3
$Ex\text{-}POEGMA_{171.4kDa}$	50.8	792	29.4	171.4	1.16	5.1 ± 1.0	1.8 ± 0.2
Index: Polymer type							
$Ex\text{-}POEGMA_{opt}$	62.3	241	29.9	54.7	1.09	4.1 ± 0.5	2.8 ± 0.7
$Ex\text{-}POEGMA_{sol}$	N/A	221	40.1	56.6	1.09	4.3 ± 0.3	3.6 ± 0.9
$Ex\text{-}PEG_{Rh}$	N/A	454	N/A	27.7	1.07	4.4 ± 1.1	1.3 ± 0.2
$Ex\text{-}PEG_{Mw}$	N/A	909	N/A	46.3	1.1	5.2 ± 1.0	2.7 ± 0.5

exendin-DBCO. To ensure that the conjugation is bioorthogonal –to avoid side-reactions of POEGMA with any internal residue in exendin, we chose to synthesize azide-terminated POEGMA copolymers. The azide moiety readily reacts with the DBCO group and does not react with any other chemical groups in exendin, yielding a conjugate with a 1:1 stoichiometry [29]. (Fig. S11).

Purification of POEGMA conjugates from unreacted agents using chromatography techniques is labor-intensive and has a low yield. To circumvent these problems, we exploited the LCST behavior of depot-forming POEGMA conjugates. The conjugates were purified in a chromatography-free manner at room temperature by simply triggering the phase transition of the conjugate by adding ammonium sulfate salt that lowers the T_t below room temperature [31], leading to phase separation of Ex-POEGMA conjugates into an insoluble coacervate. Unreacted exendin remained in the supernatant. The Ex-POEGMA coacervates were isolated by centrifugation and were then resolubilized by

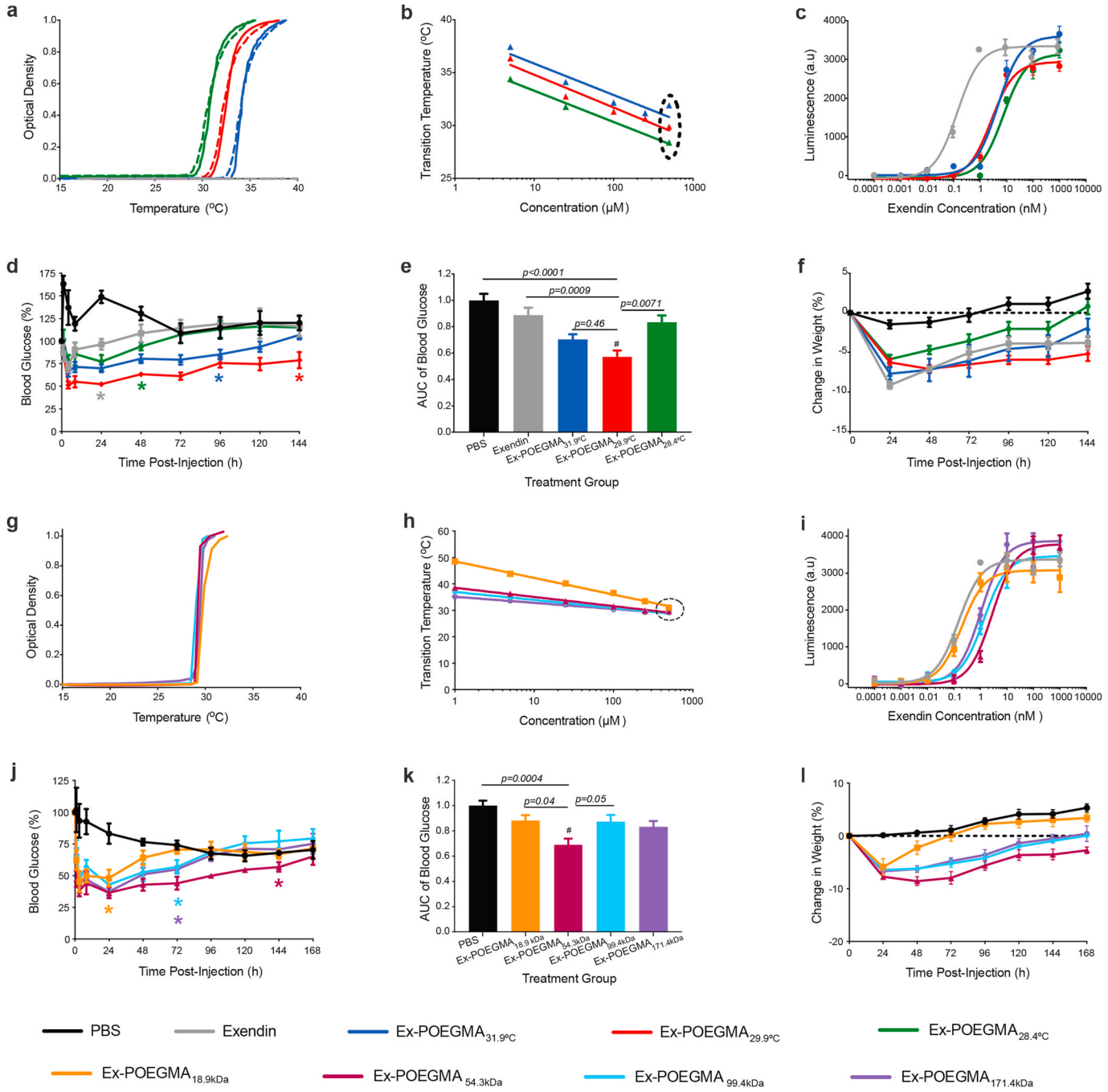

Fig. 2. Identifying an optimal Ex-POEGMA conjugate that maximizes fed blood glucose control in hyperglycemic mice. (A) The optical density of Ex-POEGMA conjugates with similar M_w but varied T_t as temperature increased (solid line) and decreased (dashed line), demonstrating the reversibility of phase behavior at 25 μM and (B) at varying concentrations to demonstrate inverse concentration-dependence of T_t. Circled data shows T_t at the injection concentration of 500 μM. (C) In vitro activity of the conjugates (n = 6). (D) Blood glucose normalized to t = 0, (E) AUC of blood glucose, and (F) percent weight change relative to weight at t = 0 after treating DIO C57BL/6J mice (n = 6) with a single s.c. injection of the treatments. (G) The optical density of Ex-POEGMA conjugates with optimal T_t but varied M_w as temperature increased, demonstrating phase behavior at 25 μM and (H) at varying concentrations to demonstrate inverse concentration-dependence of T_t. (I) In vitro activity of the conjugates (n = 6). (J) Blood glucose normalized to t = 0, (K) AUC of blood glucose, and (L) percent weight change relative to weight at t = 0 after treating DIO C57BL/6J mice (n = 6) with a single s.c. injection of the treatments. Data were analyzed by two-way repeated-measures ANOVA followed by post hoc Dunnett's multiple comparison test. *The last time point that blood glucose for treatment is significantly lower than that of PBS treated mice. The AUC for glucose exposure was analyzed using two-way ANOVA, followed by post-hoc Tukey's multiple comparison test. #The conjugate with the lowest AUC for glucose exposure. Data showed the mean ± SEM and were considered statistically significant when $p < 0.05$.

adding PBS at room temperature. Because this purification technique is not possible with soluble POEGMA and PEG conjugates, they were purified using size exclusion chromatography.

In the first phase of optimization, to identify an Ex-POEGMA conjugate with an optimal T_t, we first conjugated exendin to POEGMAs that have a varied monomer composition and hence T_t, but all of which had a near-constant M_w of ~57 kDa (Table 1; index T_t). We chose an M_w of ~57 kDa, as it was previously shown to be the M_w that maximized the PK of a soluble Ex-POEGMA conjugate (Table 1; Fig. S12) [17]. All conjugates had a low polydispersity and had a similar R_h (Table 1; Fig. S13). In addition, they showed reversible phase behavior (Fig. 2A), and the T_t of all conjugates were between 28 and 32 °C, allowing the conjugates to remain in solution at room temperature and transition into an insoluble coacervate when injected s.c. at an injection concentration of 500 μM (see circled data in Fig. 2B). The T_t of the conjugates also showed an inverse concentration-dependence (Fig. 2B), indicating that they should release from the depot into the blood in response to dilution at the depot's margins. The conjugates with a greater EG2 content had a lower T_t, as the EG2 unit is more hydrophobic than the EG3 unit. (Table 1; Fig. S14).

The rheological properties of the optimal depot-forming POEGMA ($POEGMA_{opt}$) were characterized by oscillatory rheology as a function of temperature at a polymer concentration of 3.94 mM. With an increase in temperature from 22 °C to 32 °C, both the storage (G′) and loss (G″) moduli increased sharply around the T_t of $POEGMA_{opt}$, but no crossover between G′ and G″ was observed. G″ was greater than G′ for the entire temperature range, suggesting that POEGMA is more viscous than elastic even in its coacervate phase (Fig. S15A. We also attempted to measure the rheological properties of Ex-$POEGMA_{opt}$ at the in vivo injection concentration of 500 μM. However, we suspect that the change in G′ or G″ at such a low concentration below the detection limit of the instrument as seen by the noise in the data, especially for G'. (Fig. S15B).

Next, the conjugates were tested for their ability to activate exendin's endogenous receptor, termed glucagon-like peptide 1 receptor (GLP1R), in an in vitro cell-based assay using unconjugated exendin and PBS as controls. The conjugates showed high potency in activating GLP1R (Fig. 2C) but had a higher half-maximal effective concentration (EC_{50}) than exendin due to the steric hindrance imparted by the conjugated POEGMA, consistent with the literature [17,26,29]. No significant difference was observed in the EC_{50} of depot-forming conjugates.

We then examined the fed blood glucose control provided by the Ex-POEGMA conjugates by administering them s.c. into 11-week-old male diet-induced obese (DIO) [32] C57BL/6J mice. The equivalent dose of exendin and equivalent volume of PBS were used as positive and negative controls, respectively. Mice treated with Exendin, and the conjugates had lower blood glucose levels (Fig. 2D; Fig. S16) and body weight (Fig. 2F) than the PBS-treated group. The brisk increase in blood glucose in PBS-treated mice at t = 0 was attributed to injection-related stress and was consistent across all experimental groups and studies. Exendin provided a shorter temporal duration of control than the conjugates, likely due to its short half-life [33]. The most hydrophobic conjugate tested—Ex-$POEGMA_{28.4}$—provided only modest control, possibly because it released only a small amount of drug from the depot. The Ex-$POEGMA_{29.9}$ conjugate outperformed others by providing six days of glucose control and had the lowest area under the curve (AUC) for glucose exposure (Fig. 2E), which accounts for both magnitude and duration of blood glucose reduction. This result was consistent with the literature, where the optimal T_t of an injectable elastin-like polypeptide (ELP) drug depot was also reported to be ~30 °C [26].

Having identified an Ex-POEGMA conjugate with an optimal T_t, we next identified an optimal M_w. Our strategy was to synthesize Ex-POEGMA conjugates with the optimal T_t of ~30 °C but with varying M_w (Table 1; Index M_w)—18.9 kDa, 54.3 kDa, 99.3 kDa, and 171.4 kDa (Fig. S17). As the T_t is a function of the M_w, we carried out an iterative set of polymer syntheses to create POEGMA copolymers that have the similar T_t —close to ~30°C across a range of concentrations— but varied M_w by titrating the ratio of EG2 to EG3 in the monomer feed of the synthesis, leading to the set of polymers shown in Table 1 and listed under Index: M_w. The polymers with a lower M_w had a greater mole fraction of the more hydrophobic EG2 monomer in the POEGMA copolymers and vice versa (Fig. S18). These polymers were then conjugated to exendin. The resulting Ex-POEGMA conjugates had varied R_h (Fig. S19) consistent with their different M_w, but all showed thermally reversible phase behavior (Fig. 2G). However, the T_t of the conjugates had a slightly different inverse concentration dependence, as seen by the different slopes of the log(concentration) versus T_t plots (Fig. 2H). Importantly, these plots intersected at 500 μM and ~30°C (see circled data in Fig. 2H), a temperature that fortuitously corresponds to the previously identified optimal T_t. This concentration of 500 μM was hence chosen as the injection concentration for all in vivo studies to identify the optimal M_w with constant T_t of ~30°C. No significant correlation was observed between in vitro activity of the conjugates as seen by their EC_{50} and the M_w of conjugates (Fig. 2I).

The conjugates were next administrated into 11-week-old male DIO mice (n = 6), with PBS as a negative control. Mice treated with the conjugates had lower blood glucose (Fig. 2J; Fig. S20) and body weight (Fig. 2L) than the PBS-treated group. The conjugate with the lowest M_w tested—Ex-$POEGMA_{18.9}$—controlled blood glucose only one day and had a significantly higher glucose exposure as seen by the AUC (Fig. 2K) than all other treatment groups. This data suggests that Ex-$POEGMA_{18.9kDa}$ was cleared from the circulation much faster than the other conjugates because of its significantly smaller size (R_h~2.6 vs. ~4–5 nm for the other conjugates) that is lower than the renal excretion threshold, defined as the size of serum albumin (~3.6 nm) [17,26]. This data is consistent with the literature, where PEG and ELP conjugates show a prolonged half-life at an M_w threshold of 30 kDa [34] and 35.8 kDa [26], respectively. In addition, the higher M_w Ex-POEGMA conjugates differed in their duration of glucose control. Ex-$POEGMA_{99.4}$ and Ex-$POEGMA_{171.4}$ showed modest glucose control for three days, while Ex-$POEGMA_{54.3}$ outperformed the rest with six days of glucose control and had the lowest AUC for glucose exposure. This conjugate —Ex-$POEGMA_{54.3}$— was defined as the T_t- and M_w-optimized conjugate and is subsequently referred to as Ex-$POEGMA_{opt}$ in this paper. Finally, the optimal injection dose of this conjugate was determined to be 1000 nmol kg^{-1} in a dose-escalation study, which completed the optimization process of the conjugate (Fig. S21).

2.3. *Short-term efficacy*

We next investigated the short-term efficacy of Ex-$POEGMA_{opt}$ compared to its soluble POEGMA and PEG counterparts. We synthesized the soluble counterpart of Ex-$POEGMA_{opt}$—termed Ex-$POEGMA_{sol}$—using POEGMA consisting of only EG3 monomers at the near-identical M_w of ~57 kDa (Fig. S22). In preliminary studies, we found that linear PEG has a much larger hydrodynamic size than hyperbranched POEGMA of the same M_w, resulting in conjugates with a much larger R_h at the same M_w. Because this difference could complicate side-by-side efficacy comparison of the conjugates by affecting their kidney clearance rates, we synthesized both M_w-matched and R_h-matched exendin-PEG conjugates—termed Ex-PEG_{Mw} and Ex-PEG_{Rh} (Table 1; Figs. S23–24). Ex-$POEGMA_{opt}$ reversibly phase transitioned below body temperature (Fig. 3A), allowing it to remain as a solution in a syringe at room temperature but to transition into an insoluble coacervate phase when injected s.c., as tested at a concentration of 500 μM (see circled data in Fig. 3B). In contrast, Ex-$POEGMA_{sol}$ phase-transitioned well above body temperature at all concentrations, indicating that it cannot form a depot and would remain soluble when injected into the s.c. space. Neither Ex-PEG_{Mw} nor Ex-PEG_{Rh} showed phase behavior (Fig. 3A). The conjugates showed no difference in their EC_{50} in activating the GLP1R in an in vitro, cell-based assay (Fig. 3A).

The conjugates were next administered s.c. into 11-week-old male DIO mice (n = 6) at the equivalent, optimal dose, with PBS included as a

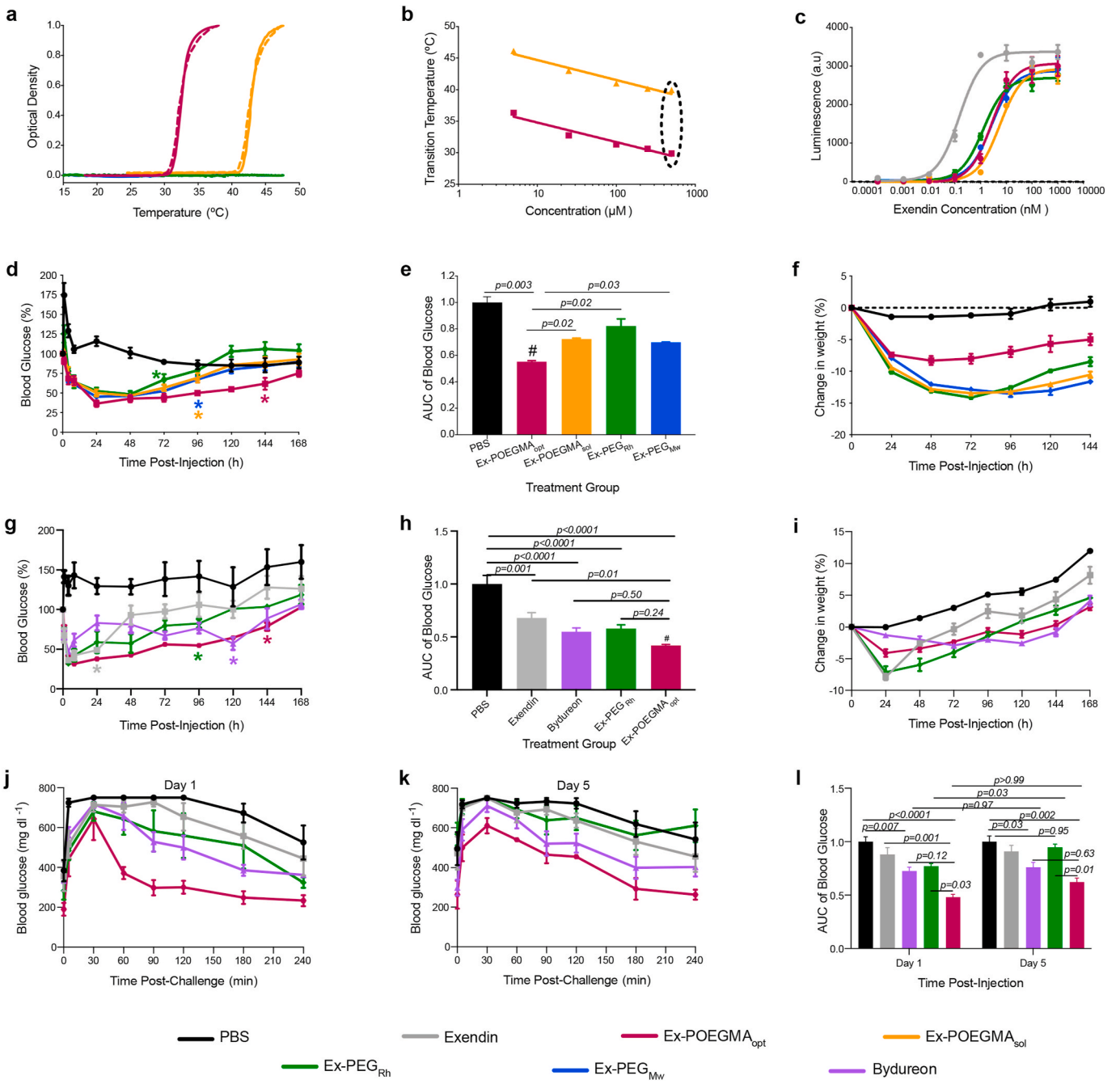

Fig. 3. Ex-POEGMA$_{opt}$ outperforms its soluble POEGMA and PEG counterparts and a clinical sustained release exendin formulation, Bydureon, in fed blood glucose and glycemic control. The optical density of treatments (A) as temperature increased and decreased, demonstrating reversible phase behavior for Ex-POEGMA$_{opt}$ and Ex-POEGMA$_{sol}$ at 25 μM and (B) at varying concentrations to demonstrate inverse concentration-dependence of T_t. Circled data show T_t at the injection concentration of 500 μM. (C) In vitro activity of the conjugates (n = 6). (D) Blood glucose normalized to t = 0, (E) AUC of blood glucose, (F) and percent weight change relative to weight at t = 0 after treating DIO mice (n = 6) with a single s.c. injection of the treatments. (G) Blood glucose normalized to t = 0, (H) AUC of blood glucose, (F) and percent weight change relative to weight at t = 0 after treating six-week-old db/db mice (n = 6) with a single s.c. injection of the treatments. An IPGTT was performed on (J) day 1 and (K) day 5 post-injection of treatments into db/db mice (n = 5), blood glucose was monitored, and (L) AUC of blood glucose was quantified. Data were analyzed by two-way repeated-measures ANOVA, followed by post hoc Dunnett's multiple comparison test. *The last time point that blood glucose for treatment is significantly lower than that of PBS treated mice. The AUC for glucose exposure was analyzed using two-way ANOVA, followed by post-hoc Tukey's multiple comparison test. #The conjugate with the lowest AUC for glucose exposure. Data showed the mean ± SEM and were considered statistically significant when $p < 0.05$.

control. Mice treated with the conjugates had lower fed blood glucose levels than the control (Fig. 3D; Fig. S25). Ex-PEG$_{Rh}$ and Ex-PEG$_{Mw}$ controlled fed blood glucose for three and four days, respectively (Fig. 3D), consistent with the literature [35]. The one-day longer glucose control provided by Ex-PEG$_{Mw}$ could be attributed to its larger size, and hence slower clearance. In accord with the literature, Ex-POEGMA$_{sol}$ also provided four days of blood glucose control [17]. In contrast, Ex-POEGMA$_{opt}$ outperformed its soluble POEGMA counterpart and the two PEGylated exendin controls by providing six days of fed blood glucose control and had the lowest glucose exposure of all conjugates (Fig. 3E), showing the enhanced efficacy provided by sustained release of the conjugate from an injectable s.c. depot. All soluble conjugates

resulted in a much sharper and more significant weight loss than Ex-POEGMA$_{opt}$ (Fig. 3F), possibly because a sudden increase in drug concentration of soluble conjugates can induce nausea and trigger transient weight loss, which is consistent with common side effects of exendin [36].

Motivated by these results, we next tested the short-term efficacy of Ex-POEGMA$_{opt}$ in a second mouse model—the db/db line—that displays more severe hyperglycemia than DIO mice. db/db mice carry mutant leptin receptor gene and have a progressive course of declining insulin secretion and hyperglycemia, similar to many humans with T2D [32]. In this study, we also compared Ex-POEGMA$_{opt}$ with Bydureon at equimolar dose, a once-weekly FDA-approved and clinically used sustained-release formulation of exendin encapsulated in poly--lactic-*co*-glycolic acid (PLGA) microspheres [37]. All treatment groups (n = 5) resulted in lower glucose levels than the PBS control (Fig. 3G; Fig. S26). Ex-POEGMA$_{opt}$, however, stood out from the competition by lowering fed blood glucose for six days. A clear trend in glucose exposure (Fig. 3H) was also observed, with Ex-POEGMA$_{opt}$ having the lowest AUC. Soluble Ex-PEG$_{Rh}$ induced a more significant weight loss than sustained-release formulations Ex-POEGMA$_{opt}$ and Bydureon (Fig. 3L), consistent with previous results.

To confirm these results, we next tested if Ex-POEGMA$_{opt}$ also provided glycemic regulation by performing an intraperitoneal (i.p.) glucose tolerance test (IPGTT) in db/db mice on days 1, 3, and 5 post-injection of the treatments. Exendin-treated mice displayed similar glucose intolerance compared to the PBS-treated mice, indicated by hyperglycemia, presumably because it cleared from circulation before IPGTTs were performed due to its short half-life (Fig. 3J-L) [33,38]. There was a clear trend in glucose exposure on days 1 and 3 (Fig. S27), with Ex-POEGMA$_{opt}$ regulating blood glucose more efficiently than Bydureon. Ex-PEG$_{Rh}$ had a progressive loss of glycemic lowering by Day 3 due to its faster clearance. Notably, Ex-POEGMA$_{opt}$ showed superior glycemic regulation to Ex-PEG$_{Rh}$ throughout the study by providing the lowest glucose exposure among the treatments. This difference was also observed when the experiment was repeated using DIO mice (Fig. S28). However, the magnitude of the difference was not as great, possibly due to the milder display of T2D allowing lower circulating Ex-PEG$_{Rh}$ concentrations to show therapeutic effect. The test time did not affect glucose exposure in the Ex-POEGMA$_{opt}$ treatment group ($p > 0.99$) (Fig. 3L), indicating that Ex-POEGMA$_{opt}$ maintained its superior glycemic regulation ability throughout the study.

2.4. *Pharmacokinetics*

We next investigated the PK of Ex-POEGMA$_{opt}$ and the PEGylated controls to better understand the differences in the short-term efficacy profiles of the treatments. We fluorescently labeled exendin, Ex-POEGMA$_{opt}$, Ex-PEG$_{Rh}$, and Ex-PEG$_{Mw}$ (Fig. S29), followed by s.c. administration into naïve DIO mice (n = 4). Fluorescence labeling was selected to prevent potential structural changes to POEGMA as it was carried out in physiological buffer. The PK parameters were determined from the drug's plasma concentration (Fig. 4A and B) and are shown in Table 2. All conjugates had much slower absorption kinetics than exendin, suggesting that the conjugates were primarily taken up from the s.c. space into the blood through the lymphatic system due to their large size [39]. Ex-POEGMA$_{opt}$ had the slowest absorption ($t_{1/2\ absorption} = 9.05 \pm 0.9$ h) among the treatments, possibly due to its amphiphilic structure and sustained release. Exendin had a fast elimination half-life and a short mean residence time ($t_{1/2\ elimination} = 2.1 \pm 0.3$ h, MRT = 4.2 ± 0.1 h), consistent with its small size (Fig. 4A) [38]. The conjugates had much longer elimination half-lives and resided longer due to their slower renal clearance (Fig. 4B). Ex-PEG$_{Rh}$ ($t_{1/2\ elimination} = 23.1 \pm 3.2$ h, MRT = 29.8 ± 2.4 h) and Ex-PEG$_{Mw}$ ($t_{1/2\ elimination} = 34.9 \pm 4.5$ h, MRT = 38.1 ± 2.3 h) prolonged exendin's circulation by ~11- and ~17-fold, respectively. The 55.6 kDa soluble Ex-POEGMA conjugate with a matching M_w as the optimal depot-forming POEGMA conjugate had a $t_{1/2\ elimination}$ of 61.2 ± 5.0 h [17]. In contrast, Ex-POEGMA$_{opt}$ outperformed all conjugates by prolonging exendin's circulation by ~46-fold ($t_{1/2\ elimination} = 97.3 \pm 3.2$ h, MRT = 59.8 ± 6.6 h), and it provided the highest drug exposure (AUC) among the treatments. These results are in accordance with the efficacy results, thus demonstrating the PK/PD benefits of sustained release from a depot. This study also allowed us to infer that the minimal effective concentration for Ex-POEGMA$_{opt}$ is 5.1 nM, which corresponds to the concentration of Ex-POEGMA$_{opt}$ after 6 days post-injection.

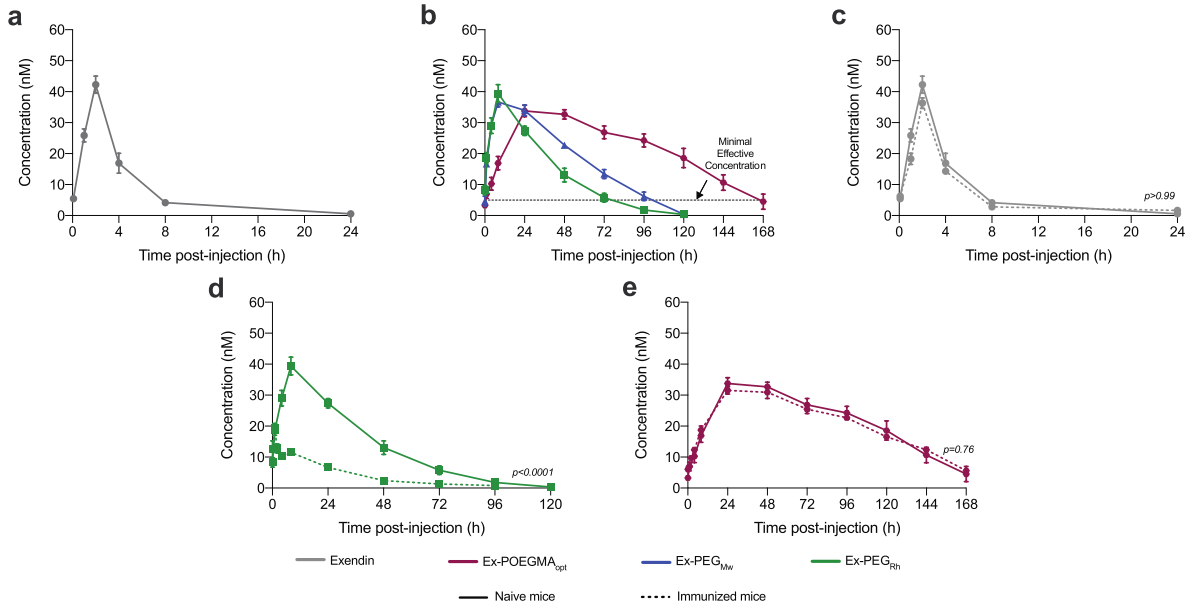

Fig. 4. Pharmacokinetics of Ex-POEGMA$_{opt}$. Fluorescently labeled (A) exendin and (B) Ex-PEG$_{Mw}$, Ex-PEG$_{Rh}$, and Ex-POEGMA$_{opt}$ were s.c. administrated into naïve male DIO C57BL/6J mice (n = 4) at 1000 nmol kg^{-1}, followed by blood collection at specified time points for 168 h to calculate drug concentration. The treatments were administrated four more times to immunize the mice and induce ADAs. At the last injection, concentrations of fluorescently labeled (C) exendin, (D) Ex-PEG$_{Rh}$, and (E) Ex-POEGMA$_{opt}$ were tracked (dotted lines). P values were shown for AUC comparison between naïve (solid line) and immunized mice for each treatment. Fluorophore concentration was 45 nmol kg^{-1}. Data represent the mean ± SEM.

Table 2
Pharmacokinetic parameters of Ex-POEGMA$_{opt}$. Pharmacokinetic parameters were calculated from the data given in Fig. 4. Data were fitted to a one-phase exponential decay curve and analyzed via non-compartmental pharmacokinetic analysis using GraphPad Prism 8 software and MRT values were calculated within WinNonlin software. Absorption phase pharmacokinetics of Ex-PEG$_{Rh}$ in immunized mice were not calculated (N/C) due to its low goodness-of-fit values. Data showed the mean ± SEM.

	Treatment	$t_{1/2\ absorption}$ (h^{-1})	$t_{1/2\ elimination}$ (h^{-1})	MRT (h)	t_{max} (h)*	C_{max} (nM)*	AUC (h x nM)
Naïve Mice	Exendin	0.65 ± 0.04	2.12 ± 0.3	4.2 ± 0.1	1.6 ± 0.1	31.7 ± 7.5	118 ± 9
	Ex-PEG$_{Rh}$	6.59 ± 0.27	23.14 ± 3.2	29.8 ± 2.4	16.6 ± 1.1	34.6 ± 1.2	1585 ± 56
	Ex-PEG$_{Mw}$	6.6 ± 0.9	34.91 ± 4.5	38.1 ± 2.2	19.5 ± 2.5	35.3 ± 2.2	2206 ± 42
	Ex-POEGMA$_{opt}$	9.1 ± 0.9	97.3 ± 3.2	59.8 ± 6.6	32.1 ± 2.9	35.8 ± 1.3	3664 ± 83
Immunized Mice	Exendin	0.77 ± 0.07	1.88 ± 0.2	4.9 ± 0.4	1.72 ± 0.1	36.9 ± 3.4	159 ± 9
	Ex-PEG$_{Rh}$	N/C	11.9 ± 2.7	24.0 ± 2.5	N/C	N/C	424 ± 17
	Ex-POEGMA$_{opt}$	12.1 ± 1.0	105.7 ± 6	70.8 ± 0.2	42.6 ± 3.2	30.3 ± 2.0	3664 ± 83

2.5. *Long-term efficacy*

We next investigated the long-term efficacy of Ex-POEGMA$_{opt}$ to understand better how the differences in PK and short-term efficacy translated into long-term management of T2D. We hypothesized that Ex-POEGMA$_{opt}$ should outperform the other exendin formulations because of its superior fed blood glucose and glycemic control and longer PK. We tested this hypothesis by administering sterile and endotoxin-free Ex-POEGMA$_{opt}$, Ex-PEG$_{Rh}$, Bydureon, exendin, and PBS (- control) s.c. into naïve six-week-old male db/db mice (n = 5) every week for eight weeks, followed by monitoring their blood glucose, changes in body weight, and glycated hemoglobin (HbA1c%) levels. We chose to monitor HbA1c %, as it is a measure of long-term T2D management because it is insensitive to daily blood glucose fluctuations and only changes as red blood cells (RBC) turn over every 40–60 days in rodents [26]. All treatments resulted in lower fed blood glucose levels (Fig. 5A; Fig. S30) and glucose exposure (Fig. 5B) than the PBS control. Exendin only had a modest and short-lived effect due to its poor circulation. Long-term treatment with Bydureon resulted in glycemic improvement (Fig. 5A and B). Ex-PEG$_{Rh}$ controlled fed blood glucose at varying degrees, with later injections providing less glycemic reduction, and resulted in a HbA1c% level that was not significantly different from PBS-treated mice ($p > 0.05$). In contrast to the other treatments, Ex-POEGMA$_{opt}$ consistently lowered fed blood glucose control after each injection and provided the lowest glucose exposure among all treatments. This profile was reflected by a lower HbA1c% in Ex-POEGMA$_{opt}$-treated mice than the levels attained with the other treatments. The sustained release formulations Bydureon and Ex-POEGMA$_{opt}$ resulted in a more moderate weight loss profile than Ex-PEG$_{Rh}$ (Fig. S31), consistent with the results after a single injection of the treatments.

2.6. *Immunogenicity*

We next tested the immunogenicity of POEGMA and compared it to PEG. PEG crosslinks the B-cell receptors (BCR) because of its linear repetitive structure, resulting primarily in a T-cell independent B-cell immune response. This response is characterized by a persistent and predominantly IgM response [40]. In humans, an IgG response is also observed in some individuals, though the mechanism of class switching is not well understood [41]. We hypothesized that POEGMA should not be immunogenic because of its hyperbranched structure, and tested this hypothesis by assessing the induction of anti-drug antibodies (ADAs) toward the full immunizing material (i.e., Ex-POEGMA$_{opt}$). We administrated sterile and endotoxin-free Ex-POEGMA$_{opt}$, Ex-PEG$_{Mw}$, exendin, and PBS (- control) s.c. into naïve DIO mice (n = 10) (see dosing and blood sampling regimen in Fig. 6A) and assessed ADAs in terms of their titer, specificity (i.e., anti-conjugate, anti-exendin, anti-PEG, or anti-POEGMA), and subtype (i.e., IgM or IgG) using a Luminex multiplexed immunoassay. Briefly, the Luminex immunoassay used drug-conjugated, fluorescently barcoded magnetic beads to capture ADAs. We coupled exendin, Ex-PEG, and Ex-POEGMA onto separate sets of beads to determine ADAs induced by the treatments. OVA versions of these beads—OVA, OVA-PEG, and OVA-POEGMA—were also coupled to separate sets of beads to use as a cross-reactivity control and to determine PEG- and POEGMA-specific ADAs, respectively. We eliminated the possibility of detecting anti-linker antibodies by synthesizing OVA-PEG and OVA-POEGMA conjugates using a different conjugation chemistry than Ex-PEG$_{Mw}$ and Ex-POEGMA$_{opt}$ (urethane linkage in OVA-based conjugates vs. strained alkyne-azide linkage in exendin-based conjugates) (Fig. S32; Table S2). Each drug-conjugated bead set had a different fluorescent barcode, allowing us to measure the signal detected by each of them when multiplexed. Mouse IgG- or

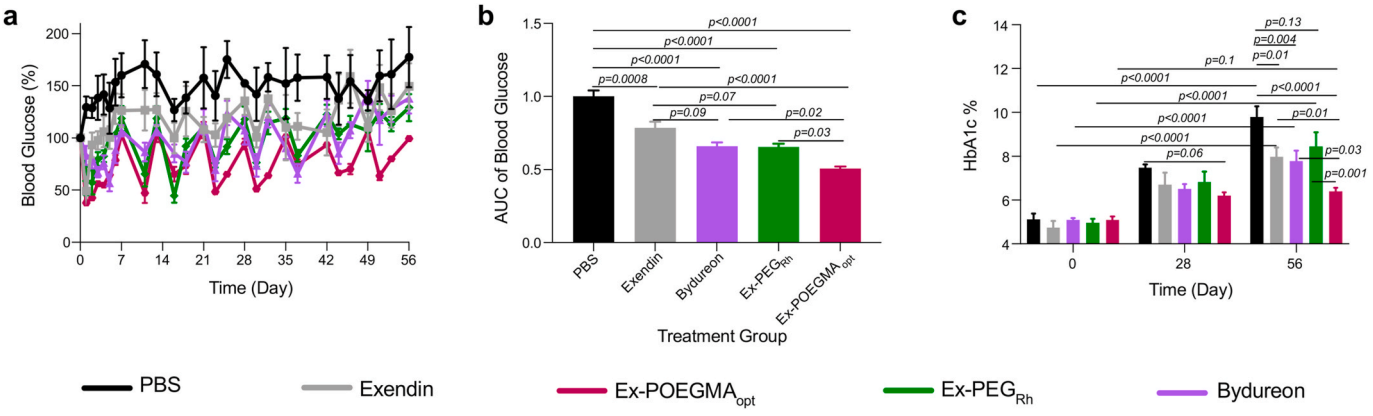

Fig. 5. Long-term efficacy of Ex-POEGMA$_{opt}$. (A) Blood glucose normalized to t = 0, and (B) AUC of blood glucose level was monitored after treating db/db (n = 5) with weekly s.c. injections of exendin, Ex-PEG$_{Rh}$, Ex-POEGMA$_{opt,}$ Bydureon, or PBS for eight weeks. (C) Percent glycated hemoglobin (Hb1Ac%). Data represent the mean ± SEM. The AUC for glucose exposure and HbA1c% were analyzed using two-way ANOVA, followed by post-hoc Tukey's multiple comparison test. Data were considered statistically significant when $p < 0.05$.

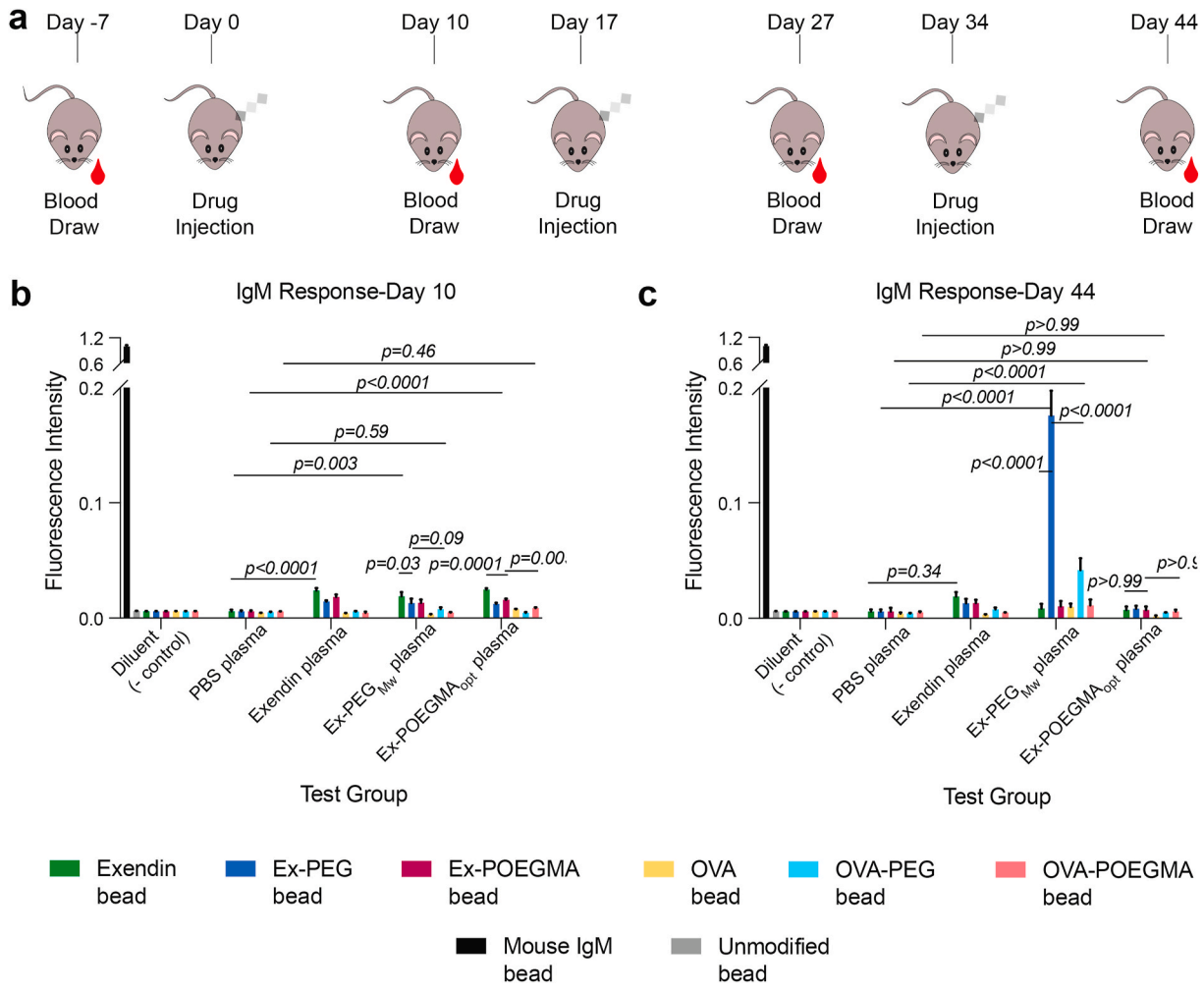

Fig. 6. Ex-POEGMA$_{opt}$ does not induce anti-POEGMA antibodies. (A) Timeline of PBS, exendin, Ex-PEG$_{Mw}$, or Ex-POEGMA$_{opt}$ administration into DIO C57BL/6J mice (n = 10) and blood collection. IgM subtype ADA response on (B) Day 10 and (C) Day 44. Blood samples were collected from mice repeatedly treated with PBS, exendin, Ex-PEG$_{Mw}$, or Ex-POEGMA$_{opt}$. ADA response was measured by a multiplexed Luminex immunoassay. Ex-PEG- and Ex-POEGMA-coupled beads were used to determine ADAs induced towards the entire conjugate (i.e., anti-exendin and anti-polymer — PEG or POEGMA). OVA-PEG- and OVA-POEGMA-coupled beads were used to determine ADAs induced towards PEG or POEGMA, respectively. The OVA-coupled beads were used as a negative control for cross-reactivity towards OVA. Data represent the mean ADA response induced in each mouse ± SEM. Data were analyzed by two-way repeated-measures ANOVA, followed by post-hoc Tukey's multiple comparison test. Data were considered statistically significant when $p < 0.05$.

IgM-coupled beads in diluent were used as positive controls, while the multiplexed beads in diluent served as a negative control. The immunoassay's optimization and validation are summarized in the Supplementary Information, and supplementary data are shown in Figs. S32–33 and Tables S2–8.

Ex-POEGMA$_{opt}$, Ex-PEG$_{Mw}$, and exendin treatments induced a transient IgM response against exendin (Fig. 6B and C). No anti-exendin IgG response was detected (Fig. S34). This data is consistent with the literature [42], where only mild induction of anti-exendin antibodies was reported in clinical trials. In contrast, Ex-PEG$_{Mw}$ induced a significant and persistent anti-PEG IgM response (Fig. 6B and C), consistent with the literature [7,8,40]. PEG specificity was indicated by the significant signal measured with both Ex-PEG and OVA-PEG beads. Anti-PEG antibodies were strictly IgM, and no class switching to IgG was observed (Fig. S34). PEG-specific IgM response increased with the number of Ex-PEG$_{Mw}$ injections (Fig. S35). Notably, the induced PEG antibodies did not bind POEGMA conjugated bead sets, indicating that POEGMA eliminates PEG antigenicity in agreement with the literature [17,18]. Strikingly, Ex-POEGMA$_{opt}$ did not induce anti-POEGMA antibodies, indicating that it is non-immunogenic.

We further tested the immunogenicity of POEGMA and compared it to PEG using OVA peptide as its conjugation partner. Briefly, OVA, OVA-PEG, OVA-POEGMA, and PBS (negative control) were repeatedly injected s.c. into naïve C57BL6/J mice (n = 10) in accordance with the timeline in Fig. 6A. The Luminex immunoassay was used to quantify the ADAs induced by the treatments with minor changes from the previous experiment. Briefly, OVA, OVA-PEG, and OVA-POEGMA coupled beads were used to quantify ADA responses to the full immunizing material, while Ex-PEG and Ex-POEGMA coupled beads were employed as irrelevant protein conjugates to measure the immune response to the polymer domains only. The exendin-coupled bead was used as a cross-reactivity control. Free, PEG-conjugated, and POEGMA-conjugated OVA induced significant anti-OVA IgG responses by Day 44 (Figs. S36A–B). The OVA-PEG conjugate induced lower titers of anti-OVA IgG than unmodified OVA (Fig. S36B). This result was attributed to the steric hindrance imparted by the PEG [6], allowing the conjugate to expose fewer OVA epitopes to the immune system. The differences in anti-OVA antibody titers were not as dramatic when POEGMA was used. We speculate that this is because POEGMA provides less steric hindrance than PEG to its conjugation partners due to its more compact architecture [43]. PEG was highly immunogenic, as seen by the high titers of PEG-specific ADAs detected in OVA-PEG-immunized mice plasma with

Ex-PEG beads (Fig. 36C and D). Similar to when exendin was the conjugation partner, PEG-specific ADAs were restricted to the IgM class (Figs. S36C–D), possibly due to the lack of T-cell help for class switching, as reported in the literature [40]. The PEG-specific IgM titer was ~60-fold higher with OVA-PEG than Ex-PEG, possibly due to the higher immunogenicity of OVA. In contrast, only a mild anti-POEGMA IgM response was detected after the first drug injection. The anti-POEGMA response was not detectable at later time points (Fig. S37D) and did not mature into an IgG response (Fig. S37H), further supporting our conclusions that POEGMA appears to be significantly less immunogenic than PEG.

Finally, we tested POEGMA's immunogenicity in an extreme case by immunizing mice with OVA-POEGMA emulsified with complete Freund's adjuvant (CFA), boosting the immune response with OVA-POEGMA emulsified with incomplete Freund's adjuvant (IFA), and comparing with OVA-PEG that administered in CFA/IFA emulsions [44]. Freund's adjuvants (FA) significantly enhance the titer and affinity of the immune response induced towards co-administered immunogens by extending their presentation, stimulating the innate immune system, and facilitating T-cell help, commonly allowing immunogens to reveal their most immunogenic state [45]. We hypothesized that POEGMA should at most induce a weak IgM immune response. We tested this hypothesis by administering PBS (- control), OVA, OVA-PEG, and OVA-POEGMA s.c. into naïve C57BL/6J mice (n = 10) in FA emulsions. Blood was collected by following the timeline in Fig. 6A, processed into plasma, and tested by a Luminex immunoassay. Strikingly, a POEGMA-specific IgM response was observed transiently and disappeared after the first injection (Figs. S38–39). In contrast, CFA/IFA emulsions magnified the anti-OVA and anti-PEG responses by ~2-fold. Notably, no change in the specificity and subtype of the immune response developed towards the treatments was detected (Fig. S37). In sum, this data confirmed the immunogenicity benefits of POEGMA over PEG even delivered with a potent adjuvant.

2.7. *Effect of ADAs on long-term efficacy*

When immunogenicity and long-term efficacy data were evaluated together, they suggested that the inferior blood glucose control with the increasing number of injections and poor HbA1c% control by Ex-PEG_{Rh} could result from anti-PEG antibody interference. To test this hypothesis, we measured the ADA levels in the plasma of long-term treated mice. To do so, plasma was collected on day 66 after 8 weekly treatments and assayed for ADAs by the Luminex immunoassay described above. Both exendin and Bydureon induced a mild anti-exendin IgM response, whereas Ex-$POEGMA_{opt}$ exhibited a weaker anti-exendin IgM response, possibly due to the non-immunogenic nature of POEGMA [19,20] and the shielding of exendin's immunogenic epitopes by POEGMA (Fig. S40A). The most striking finding of this study was the strong PEG-specific IgM and IgG responses elicited by Ex-PEG_{Rh} treatment, whereas the Ex-$POEGMA_{opt}$ did not elicit POEGMA-specific IgM or IgG antibodies (Figs. S40A–B).

Having identified the presence of anti-exendin and anti-PEG antibodies, we next investigated if the ADAs could neutralize the treatments. We analyzed the plasma of long-term treated mice for neutralizing antibodies (NAbs) using the cell-based assay developed to test the GLP1R-binding by exendin variants with minor modifications [42]. The assay design and optimization are summarized in Supplementary Information and in Table S9 and Fig. S41. The GLP1R-binding by the treatments did not change when incubated with the mice plasma, indicating that the ADAs did not neutralize the treatments (Fig. S42). This result was consistent with the results from the clinical trials of exendin, where anti-exendin ADAs did not affect its PD. We also tested if PEG-specific ADAs neutralized Ex-PEG_{Mw} by incubating the conjugate with the plasma samples of the mice immunized with Freund's adjuvant (FA) emulsion of OVA-PEG available from a previous study. Ex-PEG_{Mw} showed no change in activity (Fig. S42E), indicating that anti-PEG antibodies did not have neutralizing activity on exendin.

We finally tested the effect of ADAs on the PK of the treatments. We hypothesized that the loss of efficacy upon long-term treatment with Ex-PEG_{Mw} was due to the binding of the anti-Exendin and/or anti-PEG antibodies to the circulating drug, resulting in accelerated blood clearance and preventing it from showing efficacy [40,46]. We also hypothesized that Ex-$POEGMA_{opt}$ did not show a difference in PK among injections due to the lack of ADAs against the drug or POEGMA. To test these hypotheses, we administered s.c. sterile, endotoxin-free, and fluorescently labeled exendin, Ex-PEG_{Rh}, and Ex-$POEGMA_{opt}$ into DIO C57BL/6J (n = 4) and tracked their PK after the first (naïve mice) and fifth injection (immunized mice). Exendin did not show any difference in PK parameters between naïve and immunized mice (Fig. 4C; Table 2), indicating that the low titers of anti-exendin antibodies were not PK-altering, consistent with the literature [42]. Importantly, Ex-PEG_{Rh} showed significantly different PK profiles in naïve and immunized mice (Fig. 4D; Table 2). Ex-PEG_{Rh}'s elimination half-life was ~2-fold shorter in immunized mice compared to naïve mice ($t_{1/2\ elimination}$ = 11.4 ± 5.4 h vs. 23.1 ± 6.4 h), indicating the PK-altering nature of anti-PEG antibodies. Its absorption was also significantly lower in the immunized mice, suggesting local lymph nodes' involvement in its elimination [47]. Together, the ~4-fold lower drug exposure in immunized mice (AUC = 424 ± 35 vs. 1585 ± 112) indicated that anti-PEG immune response was responsible for the loss of efficacy in the long-term Ex-PEG_{Rh} treatment. Notably, Ex-$POEGMA_{opt}$ preserved its PK benefits after repeated administrations (Fig. 4E; Table 2), consistent with the low titer of anti-drug antibodies and the absence of anti-POEGMA antibodies elicited by long-term treatment with this conjugate.

2.8. *Histopathological effects*

We next investigated if treatment with Ex-$POEGMA_{opt}$ had any histopathological effects and compared it to Ex-PEG_{Rh}, which induces significant vacuolization in major organs, and with Bydureon, exendin, and PBS (- control) [48]. We collected kidney, pancreas, spleen, and thyroid tissues from db/db mice (n = 3) treated in the long-term study. These tissues were fixed in 10% neutral buffered formalin (NBF), processed, embedded into paraffin, sectioned, and hematoxylin and eosin (H&E) stained. The resulting tissue slides were evaluated by a veterinary pathologist experienced in toxicologic pathology. Exendin and Bydureon treatment did not induce any histopathological effects in the kidneys (Figs. S43A–C), whereas significant vacuolization was noted in the Ex-PEG_{Rh} group (Fig. S43D). These vacuolar lesions were prominent primarily within epithelial cells of the renal proximal tubules in the outer cortical region. Similarly, a low level of vacuolar change was also observed in pancreatic acinar cells of all Ex-PEG_{Rh}-treated mice (Fig. S44D), possibly because of GLP1R targeting by exendin [49] and vacuole formation by the conjugated PEG. No changes were noted within the splenic or thyroid tissues treated with Ex-PEG_{Rh} (Fig. S45). Importantly, Ex-$POEGMA_{opt}$ treatment induced no histopathological changes in the kidneys (Fig. S43E) or pancreas (Fig. S44E).

3. Discussion

Here, we report on a PEG-like injectable conjugate for the sustained delivery of biologics from a s.c. depot. This next-generation POEGMA technology platform has two key advantages over traditional PEGylation. First, to date, PEG has been conjugated with biologics to create only soluble drug formulations. The injectable, depot-forming POEGMA adds a new dimension to PEGylation by creating a drug depot under the skin that achieves sustained drug release into the circulation. Synthesizing a POEGMA conjugate of exendin that is injectable but undergoes an LCST phase transition into an insoluble coacervate phase that provides the maximal duration of release from the s.c. depot with a plasma concentration that remains above the therapeutic threshold required a stepwise optimization of the polymer composition and M_w. In the first

stage of optimization, we fixed the M_w of the POEGMA but varied the ratio of the EG2 and EG3 side chains in the monomer to create a set of copolymers that exhibit a range of T_t. Upon s.c. injection of these Ex-POEGMA conjugates in mice, we found that the T_t of these copolymers determined the depot's stability, with depots with a lower T_t leading to more stable depots, but a slower rate of release, while depots with a higher T_t had a higher rate of release with a shorter duration of release. We identified ~30 °C as the optimal T_t that balances the release rate of the conjugate (and thereby steady-state plasma concentration) with the duration of release, so that a depot with a T_t of ~30 °C provides the maximum efficacy, as by the blood glucose AUC. In the next optimization step, we fixed the T_t of the conjugate at ~30 °C while varying their M_w from ~20 to ~170 kDa. The rationale for this second stage of polymer optimization was the recognition that once the conjugate is released from the s.c. depot, the plasma half-life is controlled by renal clearance, which is a function of the M_w of the conjugate. In vivo efficacy studies revealed that a conjugate M_w of ~55 Da yielded the maximum reduction in glucose AUC compared to the PBS control. Together, these experiments identified an optimal Ex-POEGMA conjugate that has the highest efficacy, with a T_t of ~30 °C and an M_w of ~55 kDa.

Second, we previously showed that the hyperbranched structure of POEGMA does not induce a POEGMA-specific immune response. Here, we show the hyperbranched structure of POEGMA does not induce a POEGMA-specific immune response, presumably because its short OEG side chains do not crosslink B-cell receptors as PEG does [40]. Unlike PEG, which is unstructured in aqueous solvents, POEGMA self-organizes into nanoparticle-like chains due to the interfacial energy balance driven by its amphiphilicity and the repulsion forces among hydrated OEG side-chains [43]. We speculate that POEGMA's compact molecular conformation in water may effectively reduce the number of epitopes exposed to the immune system, allowing it to remain non-immunoreactive. We also showed that Ex-PEG loses its efficacy after repeated administration due to the induction of PEG-specific antibodies that reduce the PK upon repeat dose administration, preventing it from being used for long-term treatment. In contrast, the optimal injectable, depot-forming Ex-POEGMA$_{opt}$ conjugate retained its efficacy and PK benefits through repeated injections over 56 days, indicating that the injectable depot-forming POEGMA conjugate technology is a powerful approach not only to improve PK and PD but also to solve the immunogenicity problems of PEGylated therapeutics. These features allowed an optimal Ex-POEGMA depot to provide T2D management that is superior to a PEG conjugate and Bydureon. Finally, the depot-forming POEGMA technology also allows chromatography-free purification of conjugated drugs, eliminating a significant time-, labor-, and cost-intensive step in manufacturing PEGylated drugs.

The POEGMA depot technology has several advantages over other drug delivery technologies. First, POEGMA combines sustained-release and extended circulation in one molecule. Most exendin formulations, such as Bydureon, release the unmodified exendin peptide into the bloodstream that, after release, circulates only for a few hours, while the POEGMA depot releases exendin as a POEGMA conjugate that has ~46-fold longer half-life in the circulation than the unmodified peptide. The molecular design of the POEGMA conjugate also eliminates the variable drug loading seen with Bydureon [50]- and other nanoparticle-based formulations [51] as exendin is covalently conjugated with POEGMA at a known—equimolar—stoichiometry. Second, a POEGMA depot releases a steady amount of drug into circulation to achieve a desired therapeutic effect. In contrast, PLGA [50]- and nanoparticle-based sustained-release exendin formulations [51] have a burst release profile, characterized by a peak-and-valley PK [52]. Lastly, POEGMA shields exendin's immunogenic epitopes, while free exendin-releasing technologies do not have a mechanism for reduced immunogenicity, resulting in higher ADA titers and potentially altered drug efficacy. Our results supported this assertion, where no anti-exendin ADAs were detected after long-term treatment with Ex-POEGMA$_{opt}$, while Exendin and Bydureon treated mice had Exendin-specific ADAs.

In conclusion, the injectable, depot-forming POEGMA technology offers a new innovative approach to enhance PK and PD properties over PEGylation. Future plans include investigating the biodistribution of POEGMA using analytical PK methods, identifying the molecular variables that endow low immunogenicity to POEGMA conjugates, and testing the efficacy of POEGMA-drug conjugates in a large animal preclinical model as a prelude to clinical translation.

4. Materials and methods

4.1. POEGMA synthesis and purification

All materials were purchased from Millipore Sigma. Triethylene glycol methyl ether methacrylate (EG3) and diethylene glycol methyl ether methacrylate (EG2) were passed through basic alumina columns to remove inhibitors. Other materials were used as received. A catalytic complex was prepared by mixing tris(2-pyridylmethyl) amine (TPMA) and copper (II) bromide ($CuBr_2$) in ultrapure water with 18.2 MOhm resistivity at a final concentration of 0.8 M and 0.1 M, respectively. In a typical copolymerization, a Schlenk flask contained EG3 (3.5 mmol; 701.57 μl), EG2 (6.5 mmol; 1199.44 μl), azide functional polymerization initiator (0.2 M in methanol; 125 μl; see Supplementary Information for synthesis), the catalytic complex (62.5 μl), methanol (5.875 ml) and 100 mM NaCl (11.946 ml). The polymerization flask was sealed and cooled to 0 °C in an ice bath. A separate Schlenk flask contained 64 mM ascorbic acid in ultrapure water. Both flasks were purged with argon for 45 min on ice to remove oxygen. After deoxygenation, the ascorbic acid solution was continuously injected into the polymerization flask at a rate of 1 μl min^{-1} using a syringe pump under an inert atmosphere. The resulting solution was kept under vacuum to remove methanol and freeze-dried overnight. The resulting POEGMA was dissolved in acetonitrile and passed through a neutral alumina column to remove the catalytic complex. POEGMA was purified from unreacted monomer by precipitation in cold diethyl ether, followed by overnight evaporation of excess diethyl ether under vacuum.

4.2. Physical characterization of POEGMA

The M_n, M_w, and Đ of POEGMA were assessed by GPC-MALS. POEGMA was solubilized in tetrahydrofuran (THF) at 2 mg ml^{-1}, followed by filtration through a 0.22 μm Teflon syringe filter. 50 μl of the solution was separated on an Agilent PLgel mixed-C column (105 Å, 7.5 mm internal diameter x 300 mm length, and 5 μm particle size) using an Agilent 1100 analytical high-pressure liquid chromatography (HPLC). The HPLC was equipped with a UV detector operating at 254 nm (Agilent), a Dawn EOS MALS detector (Wyatt Technology), and an Optilab DSP refractometer (Wyatt Technology). The mobile phase consisted of 100 ppm butylated hydroxytoluene (BHT) in THF as a stabilizer at a 1 ml min^{-1} flow rate. Before each analysis, the MALS detector was normalized with 30 kDa polystyrene (Wyatt Technology). Refractive index increment (dn/dc) of POEGMA was calculated using ASTRA software provided with the HPLC (v. 6.0, Wyatt Technology) based on injections of known concentrations and mass, followed by data analysis for M_n, M_w, and Đ.

4.3. Structural characterization of POEGMA

.The POEGMA structure was characterized by H NMR spectroscopy using a 400 MHz Varian INOVA spectrometer and ACD/NMR software (ACD Labs). The monomer composition was defined as the molar percentage of EG2 (or EG3) content in the copolymer. The monomer composition was calculated from the integral value that corresponds to the average number of hydrogens (H) present in the OEG sidechain (b; 3.4–4.4 ppm; 6H for $EG2_{100\%}$ homopolymer; 10H for $EG3_{100\%}$ homopolymer) except the chain end-group (c; 3.5–3.3 ppm; 3H) and methylene protons (a; 4.0–4.4 ppm; 2H). The DP were calculated by

subtracting the polymerization initiator's M_w from POEGMA's M_w and dividing the resulting mass by the average M_w of a monomeric unit.

4.4. Hydrodynamic size characterization

The R_h of POEGMA and Ex-POEGMA conjugates were characterized by dynamic light scattering (DLS) in PBS at 1 mg ml^{-1} using a temperature-controlled DynaPro Plate Reader (Wyatt Technology). Samples were filtered through a 100 nm syringe filter (Whatman) prior to measurement. Ten repeat measurements of 10-s acquisitions were made at 15 °C. Data were analyzed for Raleigh spheres by applying a regularization fit using Dynamics 6.12.0.3 software (Wyatt Technology). The laser wavelength and scattering angle of the instrument were 831.95 nm and 90°, respectively.

4.5. Phase behavior characterization

The optical density of POEGMA and Ex-POEGMA conjugates were monitored at 600 nm in PBS at pH 7.4, as the temperature of the cuvet containing the samples was increased at a rate of 1 °C min^{-1} on a temperature-controlled UV–vis spectrophotometer (Cary 300 Bio, Varian Instruments). A sharp increase in the optical density with temperature indicates the occurrence of the phase transition. The T_t was defined as the temperature at the inflection point of the optical density versus the temperature curve and is calculated as the maximum of the first derivative using GraphPad Prism 8.0 software. The reversibility of the phase behavior was investigated by monitoring the optical density as the temperature was gradually decreased from a temperature above the T_t back to 15 °C.

4.6. Rheology

Data was obtained on a Anton Paar rheometer (MCR-302) with a cone-plate geometry (diameter of 24.989 mm, cone angle of 1.006°, truncation height of 49 μm). After loading 150 μl of the sample, the edge was sealed with mineral oil to prevent the evaporation of water from the sample during temperature sweep experiments. Time-temperature-superposition experiments were performed over a frequency range of 1–100 rad s^{-1} and at 5% strain amplitude over a range of temperatures from 22 °C to 46 °C. Data is reported for the angular frequency closest to 10 rad s^{-1}.

4.7. Protein expression and purification

Exendin was recombinantly expressed in E. coli from a synthetic gene in a pMA-T expression vector as an ELP fusion protein with a sortase-A recognition site (LPETG) and a polyhistidine tag, yielding exendin-LPETG-His_6-ELP (ESE). The ELP tag enables rapid non-chromatographic purification of ESE, while the LPETG peptide acts as the sortase ligation site for the ATRP initiator. Both ESE and His_6-Sortase A were available from a previous study and expressed and purified to >95% purity, as previously described [17]. The purity of all proteins was visualized by sodium dodecyl sulfate-polyacrylamide gel electrophoresis (SDS-PAGE) using 4–20% precast Tris-HCl gels (Bio-Rad), followed by staining with Simply Blue Safe Stain (Thermo Scientific) and gel densitometry analysis using Image Lab software (Bio-Rad). The ESE concentration was measured using a Bicinchoninic Acid (BCA) assay (Pierce) according to the manufacturer's instructions. The His_6-Sortase A concentration was measured by UV–visible spectroscopy on an ND-1000 Nanodrop spectrophotometer (Thermo Scientific) and the known extinction coefficient of the protein (14,440 M^{-1} cm^{-1}).

4.8. Synthesis, purification, and characterization of exendin-DBCO

A bio-orthogonal DBCO group was installed on the C-terminus of exendin by sortase A-mediated native peptide ligation, yielding exendin-DBCO. Briefly, ESE (100 μM) and His_6-Sortase A (50 μM) were reacted in the presence of triglycine-DBCO (Gly_3-DBCO) (5 mM; Click Chemistry Tools) in ligation buffer (50 mM Tris, 150 mM NaCl, and 10 mM $CaCl_2$; pH 7.5) at room temperature for 16 h. Exendin-DBCO was purified from the reaction mixture by reverse immobilized metal affinity chromatography using an AKTA Purifier (GE Healthcare) equipped with a photodiode array operating at 220 and 280 nm and a HisTrap HP (GE Healthcare) column. Exendin-DBCO was collected in the flow-through as it was the only species that did not carry an oligohistidine tag, and hence did not bind to the resin. Exendin-DBCO was concentrated by ultrafiltration using Centricon 70 (Millipore Sigma) filters with a 3000 Da molecular weight cut-off (MWCO), followed by dialysis into cold water and lyophilization. Stoichiometric (1:1) attachment of DBCO to exendin was confirmed by Matrix-Assisted Laser Desorption/Ionization-Time-of-Flight mass spectroscopy (MALDI-TOF-MS).

4.9. Synthesis and purification of exendin conjugates

Exendin-DBCO was conjugated to azide-functional POEGMA or PEG via the strain-promoted alkyne-azide click reaction. Exendin-DBCO and azide-functional POEGMA or PEG were dissolved in PBS at a 1.05:1 ratio and reacted overnight at 4 °C. Depot-forming Ex-POEGMA conjugates were purified by triggering their LCST phase transition by the addition of ammonium sulfate to a final concentration of 0.1 M. The dense phase that contained the conjugate was recovered by centrifugation at 21,000 g for 15 min at room temperature, the supernatant was removed, and the conjugate was dissolved in PBS at 4 °C. The last two steps were repeated twice to obtain conjugates with >99% purity, as verified by SDS-PAGE and HPLC. In the final step, the conjugate was dissolved in ultra-pure water and lyophilized. Soluble Ex-POEGMA and Ex-PEG conjugates were purified by a single round of size exclusion chromatography (SEC) using an AKTA purifier equipped with a photodiode array detector operating at 220 and 280 nm and a HiLoad 16/600 Superdex 75 pg column (GE Healthcare) at 4 °C using PBS as the mobile phase. The purified conjugates were concentrated by ultrafiltration using Amicon filters (Millipore Sigma) with a 3000 Da MWCO, followed by dialysis into the water at 4 °C overnight and lyophilization.

4.10. Physical characterization of exendin conjugates

The conjugates were characterized in terms of their M_n, M_w, and Đ by SEC-MALS using an Agilent 1260 analytical HPLC equipped with a UV detector operating at 280 nm (Agilent), a DAWN HELEOS II MALS detector (Wyatt Technology), and an Optilab T-rEX refractive index detector (Wyatt Technology). The DAWN HELEOS II MALS detector was annually calibrated in toluene and normalized with 2 mg ml^{-1} bovine serum albumin (Pierce) before each analysis. The exendin conjugates were dissolved in 10 mM phosphate buffer at pH 7.4, followed by filtration through a 100 nm syringe filter (Whatman). 50 μl of the conjugate was separated on a Shodex KW-803 column (8 mm internal diameter x 300 mm length, and 5 μm particle size) at a flow rate of 0.5 ml min^{-1}. The mobile phase was 30% (v/v) methanol in 10 mM phosphate buffer at pH 7.4. Data were analyzed for M_n, M_w, and Đ using ASTRA software (v. 7.0, Wyatt Technology).

4.11. In vitro activity of exendin variants

The activity of exendin and its conjugates with POEGMA and PEG were measured by GLP1R activation in a cell-based assay, which increases intracellular cyclic adenosine monophosphate (cAMP) levels upon activation of the GLP1R by exendin or its conjugates. Intracellular cAMP concentrations were quantified by treating Human Embryonic Kidney 293 cells recombinantly expressing GLP1R and luciferase fused cAMP (HEK293/CRE-Luc/GLP1R) with exendin variants. This recombinant cell line was a generous gift from Timothy Kieffer (University of British Columbia) and authenticated via short tandem repeat (STR)

analysis by the American Type Culture Collection (ATCC).

HEK293/CRE-Luc/GLP1R cells were cultured in high glucose Dulbecco's Minimal Essential Medium (DMEM) (Gibco), supplemented with 10% fetal bovine serum (Hyclone), 400 μg ml^{-1} G418 (Thermo Fisher), and 200 μg ml^{-1} Hygromycin B (Invitrogen). Cells were subcultured at least once before the assay at approximately 80% confluency. One day before performing the assay, cells were seeded without antibiotics in phenol red-free DMEM (Gibco) on 96-well plates at 25,000 cells per well in 90 μl media followed by incubation at 37 °C under 5% CO2 atmosphere overnight. Exendin conjugates (20 μM in PBS) were incubated with dipeptidyl peptidase IV (DPP-IV, Prospec Bio) to expose an active N-terminus for 16 h at room temperature. DPP-IV amount was 2.5 mass % of exendin present in the conjugates. On the day of the assay, exendin (Santa Cruz Biotechnology) was dissolved to a final concentration of 20 μM in PBS. Logarithmic serial dilutions were made for exendin variants in PBS using unmodified exendin as a positive control. 10 μl of each dilution was transferred to wells (n = 6), yielding a concentration range of 10^{-13}–10^{-6} M. The plates were then incubated at 37 °C for 5 h, followed by equilibration with room temperature for 1 h. Next, 100 μl Bright-Glo™ reagent (Promega) was added to the wells and incubated for 2 min, followed by measuring luminescence using a Victor plate reader (PerkinElmer). Data were analyzed for net luminescence by subtracting PBS-treated wells' mean luminescence (negative control) from exendin variants. The effective half-maximal dose (EC_{50}) of each exendin variant was determined by fitting the dose-response curve to a four-parameter logistic, nonlinear regression model using GraphPad Prism 8 software.

4.12. *In vivo studies*

In vivo studies were conducted under protocols approved by Duke Institutional Animal Care and Use Committee (IACUC) by employing six-week-old male C57BL/6J (Jackson Laboratories; stock no. 000664) or B6.BKS(D)-$Lepr^{db}$/J mice (db/db; Jackson Laboratories; stock no: 000697). C57BL/6J mice were kept on a 60 kilocalorie (kcal) % fat diet (Research Diets Inc.; #D12492i) for at least five weeks before and during the experiments unless otherwise noted, yielding DIO mice. Six-week-old male db/db mice were fed a standard rodent diet (LabDiet 5001) and acclimatized to facilities for one week before the experiments. Mice were group-housed under controlled photoperiod with 12 h light and 12 h dark cycles and acclimated to the facility for a week before the start of experiments. Mice had ad libitum access to water and food unless otherwise noted.

All samples were endotoxin purified using endotoxin removal columns (Pierce) and sterilized using a 0.22 μm Acrodisc filter with a Mustang E membrane (Pall Corporation). The final endotoxin amount was tested below 5 EU per kg mouse body weight using the Endosafe nexgen-PTS instrument and cartridges (Charles River). For the samples used in the long-term efficacy experiments, a more stringent endotoxin limit of a maximum of 0.2 EU per kg mouse body weight was used.

4.13. *Fed blood glucose measurements*

In the short-term efficacy experiments, the fed blood glucose was measured after a single s.c. injection of the treatments. On the day of injection, the tail was sterilized with alcohol pads (BD). The first drop of blood collected from a tiny incision on the tail vein was wiped off. The second drop of blood was used to measure fed blood glucose using a hand-held glucometer (AlphaTrack, Abbott). The treatments were solubilized in PBS and kept on ice before injection to prevent phase transition, followed by s.c. administration into mice. Bydureon was prepared for injection according to the manufacturer's instructions. Fed blood glucose levels were measured 24 h and immediately before injection, at 1-, 4-, and 8-h post-injection, and every 24 h after that until no significant effect of treatments on fed blood glucose was observed. Body weight was tracked daily. In the long-term efficacy experiment, fed blood glucose and body weight were tracked every three days.

4.14. *IPGTT*

The glycemic regulation ability of treatments was assessed by performing three IPGTTs after a single s.c. injection. Db/db mice were used during the first week of the long-term pharmacodynamics study. On day 0, the treatments were administrated into the mice at an equivalent dose (1000 nmol per kg bodyweight) and concentration (500 μM) using the equivalent injection volume of PBS as a negative control. Bydureon was prepared for injection according to the manufacturer's instructions. On the day of the IPGTT (Day 1, 3, and 5), mice were fasted 6 h before the glucose challenge by an i.p. injection of 1.5 g kg^{-1} of glucose (Sigma) followed by blood glucose monitoring at 5-, 15-, 30-, 60-, 90-, 120-, 180- and 240 min.

4.15. *HbA1c% measurement*

In long-term pharmacodynamics experiments, db/db mice (n = 5) were repeatedly injected with the treatments at an equivalent dose (1000 nmol per kg body weight in PBS) and concentration (500 μM) every seven days over 56 days using an equivalent injection volume of PBS as a negative control. Bydureon was prepared for injection according to the manufacturer's instructions. HbA1c% was measured on Day 0 before injection, Day 28, and Day 56 using DCA Vantage Analyzer and DCA HbA1c reagent kit (Siemens).

4.16. *Pharmacokinetics*

Exendin variants were labeled with a fluorophore to track their pharmacokinetics. Briefly, Alexa Fluor 488 NHS ester (Pierce) was reacted with exendin variants (5 mg ml^{-1}) at a 5:1 M ratio in PBS for 1 h at room temperature. Unreacted excess fluorophore was removed by dialysis into the water at 4 °C using membranes with a 3000 Da MWCO (Pierce), verified by HPLC. The labeling efficiency was calculated from UV–vis spectroscopy using an ND-1000 Nanodrop spectrophotometer (Thermo Scientific).

The fluorophore-labeled treatments were administered into DIO C57BL/6J mice via a single s.c. injection at 1000 nmol kg^{-1} (45 nmol kg^{-1} fluorophore). Ten μl of blood was collected from a tiny incision on the tail vein into tubes containing 90 μl of 1000 U ml-1 heparin (Sigma) at 5-min, 1-, 2-, 4-, 8-, 24-, 48-, 72-, 96-, 120-, 144- and 168-h. Blood samples were centrifugated at 1600 g at 4 °C for 15 min for plasma. Fluorophore concentration in plasma samples was detected by a Victor plate reader (PerkinElmer) at 485 nm (excitation) and 535 nm (emission). PK parameters were derived by plotting the drug's plasma concentration as a function of time and fitting it to a non-compartmental PK model for the absorption and elimination phases using GraphPad Prism software. The absorption phase described the time between injection at 0-h and t_{max}, where the drug concentration was maximum. The elimination phase described the time after t_{max}. t_{max} was calculated from equation $t_{max} = \left(\frac{2.303}{k_a - k_e}\right) * \log\frac{k_a}{k_e}$, where k_a and k_e were the apparent absorption and elimination rate constants. The rate constants were determined from the linear regression slope of the log (drug concentration) versus time graph using equation $k = -2.303 * \text{slope}$. Half-lives of treatments in each phase were determined from the equation $t_{1/2} = \frac{0.693}{k}$. Since the PK profiling is complex and identification of elimination process is somewhat arbitrary, we also calculated mean residence time (MRT = AUMC/AUC), a model-independent parameter, using non-compartmental approach within WinNonlin software. The maximum drug concentration (C_{max}) was calculated at t_{max}. Minimal effective conjugate concentration was calculated by triangulating the concentration values based on the duration of blood glucose control determined in short-term efficacy experiments in DIO mice.

ADAs' effect on the PK was investigated by weekly administering the

fluorophore-labeled treatments into the DIO C57BL/6J mice five times. Blood samples were collected after the first and last injection, and PK parameters were determined as described above.

4.17. Immunogenicity

We tested the immunogenicity of POEGMA and compared it to that of PEG in three sets of immunogenicity experiments. In the first set, sterile and endotoxin-free exendin, Ex-PEG_{Mw}, and Ex-$POEGMA_{opt}$ were s.c. administrated into 7-week-old C57BL/6J mice (n = 10) at an equivalent dose (1000 nmol kg^{-1}) and concentration (500 μM). In the second set of experiments, mice were injected with OVA (Invivogen), OVA-PEG_{10K}, and OVA-$POEGMA_{10K}$ at 9.6 nmol kg^{-1} (100 μl). In the final set, OVA, OVA-PEG_{10K}, and OVA-$POEGMA_{10K}$ were emulsified in an equal volume of sterile CFA/IFA (Invivogen) and then administrated into 7-week-old C57BL/6J mice (n = 10) at 9.6 nmol kg^{-1} (100 μl). CFA was used for the first injections, while IFA was used for the subsequent injections. An equal injection volume of PBS (or PBS emulsified in CFA or IFA) was used as a negative control in all experimental sets. All drugs were administrated into mice every 17 days three times (Day 0, 17, and 34). The injection site was the loose skin over the shoulders and was kept the same across the injections. Blood samples were collected seven days before the first injection (Day −7) and ten days after each injection (Day 10, 27, and 44), followed by plasma isolation via centrifugation at 4 °C at 1600 g for 15 min, aliquoting on ice, and storage at −80 °C until analysis.

4.18. Analysis of ADA response

ADAs were analyzed using a Luminex multiplex immunoassay. Assay design, optimization, and validation were given in Supplementary Information. The plasma samples of mice treated with exendin variants were diluted 200-fold in 0.2% (w/v) I-Block protein-based blocking reagent (Thermo Scientific) in PBS (Hyclone), defined as the assay buffer. The plasma samples of mice treated with OVA variants (n = 10) were diluted 500- and 10,000-fold in the assay buffer for IgM and IgG analysis, respectively.

In a typical LMI assay, 50 μl of the diluted plasma samples (n = 3) were transferred to a black, round-bottom 96-well-plate (Corning). Next, spectrally distinct exendin-, Ex-PEG-, Ex-POEGMA-, OVA-, OVA-PEG-, and OVA-POEGMA-coupled magnetic bead sets were mixed at a concentration of 2500 beads per 50 μl per set. 50 μl of the resulting solution was distributed to the wells of a 96-well plate and incubated for 1 h on an orbital shaker to capture ADAs present in the plasma samples. After incubation, 96-well-plate was placed on a magnetic ring stand (Invitrogen) and incubated for 60 s for separation to occur. The supernatant was discarded, and wells were washed with 100 μl of the assay buffer twice. The resulting magnetic bead-ADA complexes were incubated with 100 μl of 5 μg ml^{-1} R-Phycoerythrin-conjugated goat anti-mouse IgG (Jackson Immunoresearch; #115-115-164) for 30 min to detect IgG subtypes of ADAs. 100 μl of 5 μg ml^{-1} biotin-conjugated goat anti-mouse IgM (Jackson Immunoresearch; #115-065-075) was used to detect IgM subtypes of ADAs, followed by washes, incubation with 100 μl of 7.5 μg ml^{-1} streptavidin-R-phycoerythrin (SAPE; Invitrogen) for 30 min, and a final round of washes. Mouse IgG- or IgM-coupled magnetic beads were used as positive controls. They were incubated with 100 μl of 0.25 μg ml^{-1} R-Phycoerythrin-conjugated goat anti-mouse IgG or 0.114 μg ml^{-1} biotin-conjugated goat anti-mouse IgM, followed by 0.171 μg ml^{-1} SAPE. The negative control was the drug-coupled bead mixture in the assay buffer. Finally, magnetic beads were suspended in 100 μl of assay buffer, followed by measuring mean fluorescence signal intensity (MFI) using MAGPIX (Luminex) instrument. The average MFI value of each plasma sample and treatment was computed with no exception for outliers. Mouse plasma samples were considered ADA-positive if the average MFI for any given bead type was above the background (see Supplementary Information). MFI of each plasma sample for any given bead type was normalized to the positive control.

4.19. Histology

The db/db mice used in the long-term efficacy experiment were sacrificed, followed by collecting the organs into 10% neutral-buffered formalin (NBF). After fixation in 10% NBF, the tissues were trimmed, paraffin embedded, and sectioned at 5 μm for light microscopy, followed by H&E staining.

4.20. Statistical Analysis and safety

In all the animal studies, animals were randomized, and group sizes were estimated using open-source G*Power software based on the literature, and adequate power was ensured to detect differences. Data were presented as mean ± standard error of the mean (SEM) unless otherwise noted differently. Blood glucose data were plotted as a function of time using raw values and normalized values. Normalization reflects the percent change in blood glucose with treatment. It was calculated by dividing raw the fed blood glucose measurement at any given time point by an average value of fed blood glucose levels measured 24 h (t = −24 h) and immediately before injection (t = 0 h). Blood glucose and body weight data were analyzed using two-way repeated-measures analysis of variance (ANOVA) followed by post hoc Dunnett's multiple comparison test. The AUC for glucose exposure was quantified for each subject using the trapezoid rule and analyzed using two-way ANOVA, followed by post-hoc Tukey's multiple comparison test. HbA1c% and ADA data were analyzed using two-way ANOVA, followed by post-hoc Tukey's multiple comparison test. A test was considered significant if the p-value is < 0.05 (*$p < 0.05$; **$p < 0.01$; ***$p < 0.001$; ****$p < 0.0001$; ns: $p > 0.05$). GraphPad Prism 8.0 was used for all statistical analyses. No unexpected or unusually high safety hazards were encountered.

Data and material availability

All data is available in the manuscript or the supplementary materials.

Author contributions

I.O. and A.C. conceived and designed the research. I.O., A.S., P.S., N. Z., X.L., and G.Y. performed the experiments. J.H.C., J.E.C., D.A.D., I.S., J.I.E., and S.L.G. contributed to experimental design. I.O. and A.C. interpreted the results and wrote the manuscript. All authors participated in the discussion of the data and commented on the manuscript.

Declaration of competing interest

The authors declare that they have no known competing financial interests or personal relationships that could have appeared to influence the work reported in this paper.

Data availability

Data will be made available on request.

Acknowledgments

We thank Dr. Peter Silinski at the Duke Chemistry Mass Spectrometry Facility for mass spectrometry analyses on the monomers and the polymerization initiator. We also thank the Duke University School of Medicine for the use of the Proteomics and Metabolomics Shared Resource, which provided analysis on the stoichiometry of DBCO installment to exendin, and Duke Immune Profiling Core (DIPC) at Duke University Center for AIDS Research (CFAR) for the use of Luminex

MAGPIX. A.C. acknowledges the support of the NIH through grant R01DK124276. S.L.C. acknowledges the support of the U.S. Army Research Office grant W911NF-20-2-0182.

Appendix A. Supplementary data

Supplementary data to this article can be found online at https://doi.org/10.1016/j.biomaterials.2022.121985.

References

[1] B. Leader, Q.J. Baca, D.E. Golan, Protein therapeutics: a summary and pharmacological classification, Nat. Rev. Drug Discov. 7 (2008) 21–39.
[2] K. Fosgerau, T. Hoffmann, Peptide therapeutics: current status and future directions, Drug Discov. Today 20 (2015) 122–128.
[3] M.R. Turner, S.V. Balu-Iyer, Challenges and opportunities for the subcutaneous delivery of therapeutic proteins, J. Pharmaceut. Sci. 107 (2018) 1247–1260.
[4] Y. Vugmeyster, X. Xu, F.P. Theil, L.A. Khawli, M.W. Leach, Pharmacokinetics and toxicology of therapeutic proteins: advances and challenges, World J. Biol. Chem. 3 (2012) 73–92.
[5] I. Ekladious, Y.L. Colson, M.W. Grinstaff, Polymer–drug conjugate therapeutics: advances, insights and prospects, Nat. Rev. Drug Discov. 18 (2019) 273–294.
[6] J.M. Harris, R.B. Chess, Effect of pegylation on pharmaceuticals, Nat. Rev. Drug Discov. 2 (2003) 214–221.
[7] N.J. Ganson, S.J. Kelly, E. Scarlett, J.S. Sundy, M.S. Hershfield, Control of hyperuricemia in subjects with refractory gout, and induction of antibody against poly(ethylene glycol) (PEG), in a phase I trial of subcutaneous PEGylated urate oxidase, Arthritis Res. Ther. 8 (2006) R12.
[8] M.S. Hershfield, N.J. Ganson, S.J. Kelly, E.L. Scarlett, D.A. Jaggers, J.S. Sundy, Induced and pre-existing anti-polyethylene glycol antibody in a trial of every 3-week dosing of pegloticase for refractory gout, including in organ transplant recipients, Arthritis Res. Ther. 16 (2014) R63.
[9] R.P. Garay, R. El-Gewely, J.K. Armstrong, G. Garratty, P. Richette, Antibodies against polyethylene glycol in healthy subjects and in patients treated with PEG-conjugated agents, Expet Opin. Drug Deliv. 9 (2012) 1319–1323.
[10] A.W. Richter, E. Akerblom, Polyethylene glycol reactive antibodies in man: titer distribution in allergic patients treated with monomethoxy polyethylene glycol modified allergens or placebo, and in healthy blood donors, Int. Arch. Allergy Appl. Immunol. 74 (1984) 36–39.
[11] Q. Yang, T.M. Jacobs, J.D. McCallen, D.T. Moore, J.T. Huckaby, J.N. Edelstein, S. K. Lai, Analysis of pre-existing IgG and IgM antibodies against polyethylene glycol (PEG) in the general population, Anal. Chem. 88 (2016) 11804–11812.
[12] N.J. Ganson, T.J. Povsic, B.A. Sullenger, J.H. Alexander, S.L. Zelenkofske, J. M. Sailstad, C.P. Rusconi, M.S. Hershfield, Pre-existing anti–polyethylene glycol antibody linked to first-exposure allergic reactions to pegnivacogin, a PEGylated RNA aptamer, J. Allergy Clin. Immunol. 137 (2016) 1610–1613, e1617.
[13] J.K. Armstrong, G. Hempel, S. Koling, L.S. Chan, T. Fisher, H.J. Meiselman, G. Garratty, Antibody against poly(ethylene glycol) adversely affects PEG-asparaginase therapy in acute lymphoblastic leukemia patients, Cancer 110 (2007) 103–111.
[14] J.J. Verhoef, J.F. Carpenter, T.J. Anchordoquy, H. Schellekens, Potential induction of anti-PEG antibodies and complement activation toward PEGylated therapeutics, Drug Discov. Today 19 (2014) 1945–1952.
[15] P. Zhang, F. Sun, S. Liu, S. Jiang, Anti-PEG antibodies in the clinic: current issues and beyond PEGylation, J. Contr. Release : official journal of the Controlled Release Society 244 (2016) 184–193.
[16] C.J. Fee, Size comparison between proteins PEGylated with branched and linear poly(ethylene glycol) molecules, Biotechnol. Bioeng. 98 (2007) 725–731.
[17] Y. Qi, A. Simakova, N.J. Ganson, X. Li, K.M. Luginbuhl, I. Ozer, W. Liu, M. S. Hershfield, K. Matyjaszewski, A. Chilkoti, A brush-polymer/exendin-4 conjugate reduces blood glucose levels for up to five days and eliminates poly(ethylene glycol) antigenicity, Nature Biomedical Engineering 1 (2016), 0002.
[18] D.Y. Joh, Z. Zimmers, M. Avlani, J.T. Heggestad, H.B. Aydin, N. Ganson, S. Kumar, C.M. Fontes, R.K. Achar, M.S. Hershfield, A.M. Hucknall, A. Chilkoti, Architectural modification of conformal PEG-bottlebrush coatings minimizes anti-PEG antigenicity while preserving stealth properties, Advanced Healthcare Materials 8 (2019), 1801177.
[19] I. Ozer, G. Kelly, R. Gu, X. Li, N. Zakharov, P. Sirohi, S.K. Nair, J.H. Collier, M. S. Hershfield, A.M. Hucknall, A. Chilkoti, Polyethylene glycol-like brush polymer conjugate of a protein drug does not induce an antipolymer immune response and has enhanced pharmacokinetics than its polyethylene glycol counterpart, Adv. Sci. (2022), e2103672.
[20] I. Ozer, G.A. Pitoc, J.M. Layzer, A. Moreno, L.B. Olson, K.D. Layzer, A.M. Hucknall, B.A. Sullenger, A. Chilkoti, PEG-like brush polymer conjugate of RNA aptamer that shows reversible anticoagulant activity and minimal immune response, Adv. Mater. 34 (2022), e2107852.
[21] B. Zhang, H. Tang, P. Wu, Depth analysis on the unusual multistep aggregation process of oligo(ethylene glycol) methacrylate-based polymers in water, Macromolecules 47 (2014) 4728–4737.
[22] S. Sun, P. Wu, On the thermally reversible dynamic hydration behavior of oligo (ethylene glycol) methacrylate-based polymers in water, Macromolecules 46 (2013) 236–246.
[23] N. Badi, Non-linear PEG-based thermoresponsive polymer systems, Prog. Polym. Sci. 66 (2017) 54–79.
[24] J.-F. Lutz, Polymerization of oligo(ethylene glycol) (meth)acrylates: toward new generations of smart biocompatible materials, J. Polym. Sci. Polym. Chem. 46 (2008) 3459–3470.
[25] A. Simakova, S.E. Averick, D. Konkolewicz, K. Matyjaszewski, Aqueous ARGET ATRP, Macromolecules 45 (2012) 6371–6379.
[26] K.M. Luginbuhl, J.L. Schaal, B. Umstead, E.M. Mastria, X. Li, S. Banskota, S. Arnold, M. Feinglos, D. D'Alessio, A. Chilkoti, One-week glucose control via zero-order release kinetics from an injectable depot of glucagon-like peptide-1 fused to a thermosensitive biopolymer, Nat Biomed Eng 1 (2017).
[27] A. Ramírez-Jiménez, K.A. Montoya-Villegas, A. Licea-Claverie, M.A. Gónzalez-Ayón, Tunable thermo-responsive copolymers from DEGMA and OEGMA synthesized by RAFT polymerization and the effect of the concentration and saline phosphate buffer on its phase transition, Polymers 11 (2019) 1657.
[28] I. Ozer, A. Chilkoti, Site-Specific and Stoichiometric Stealth Polymer Conjugates of Therapeutic Peptides and Proteins, Bioconjugate Chemistry, 2016.
[29] Y. Pang, J. Liu, Y. Qi, X. Li, A. Chilkoti, A modular method for the high-yield synthesis of site-specific protein-polymer therapeutics, Angew Chem. Int. Ed. Engl. 55 (2016) 10296–10300.
[30] B.J. J., B. Jayanta, C. Ashutosh, A noncanonical function of sortase enables site-specific conjugation of small molecules to lysine residues in proteins, Angew. Chem. Int. Ed. 54 (2015) 441–445.
[31] K. Bebis, M.W. Jones, D.M. Haddleton, M.I. Gibson, Thermoresponsive behaviour of poly[(oligo(ethyleneglycol methacrylate)]s and their protein conjugates: importance of concentration and solvent system, Polym. Chem. 2 (2011) 975–982.
[32] M. Kleinert, C. Clemmensen, S.M. Hofmann, M.C. Moore, S. Renner, S.C. Woods, P. Huypens, J. Beckers, M.H. de Angelis, A. Schürmann, M. Bakhti, M. Klingenspor, M. Heiman, A.D. Cherrington, M. Ristow, H. Lickert, E. Wolf, P.J. Havel, T. D. Müller, M.H. Tschöp, Animal models of obesity and diabetes mellitus, Nat. Rev. Endocrinol. 14 (2018) 140–162.
[33] A.A. Young, B.R. Gedulin, S. Bhavsar, N. Bodkin, C. Jodka, B. Hansen, M. Denaro, Glucose-lowering and insulin-sensitizing actions of exendin-4: studies in obese diabetic (ob/ob, db/db) mice, diabetic fatty Zucker rats, and diabetic rhesus monkeys (Macaca mulatta), Diabetes 48 (1999) 1026.
[34] P. Caliceti, F.M. Veronese, Pharmacokinetic and biodistribution properties of poly (ethylene glycol)–protein conjugates, Adv. Drug Deliv. Rev. 55 (2003) 1261–1277.
[35] D. Tang, H. Tian, J. Wu, J. Cheng, C. Luo, W. Sai, X. Song, X. Gao, W. Yao, C-terminal site-specific PEGylated Exendin-4 analog: a long-acting glucagon like Peptide-1 receptor agonist, on glycemic control and beta cell function in diabetic db/db mice, J. Pharmacol. Sci. 138 (2018) 23–30.
[36] S.E. Kanoski, L.E. Rupprecht, S.M. Fortin, B.C. De Jonghe, M.R. Hayes, The role of nausea in food intake and body weight suppression by peripheral GLP-1 receptor agonists, exendin-4 and liraglutide, Neuropharmacology 62 (2012) 1916–1927.
[37] C. Ballav, S. Gough, Bydureon: long-acting exenatide for once-weekly injection, Prescriber 23 (2012) 30–33.
[38] B.R. Gedulin, P.A. Smith, C.M. Jodka, K. Chen, S. Bhavsar, L.L. Nielsen, D. G. Parkes, A.A. Young, Pharmacokinetics and pharmacodynamics of exenatide following alternate routes of administration, Int. J. Pharm. 356 (2008) 231–238.
[39] W.F. Richter, S.G. Bhansali, M.E. Morris, Mechanistic determinants of biotherapeutics absorption following SC administration, AAPS J. 14 (2012) 559–570.
[40] Q. Yang, S.K. Lai, Anti-PEG Immunity: Emergence, Characteristics, and Unaddressed Questions, vol. 7, Wiley Interdiscip Rev Nanomed Nanobiotechnol, 2015, pp. 655–677.
[41] G.T. Kozma, T. Shimizu, T. Ishida, J. Szebeni, Anti-PEG antibodies: properties, formation, testing and role in adverse immune reactions to PEGylated nano-biopharmaceuticals, Adv. Drug Deliv. Rev. 154–155 (2020) 163–175.
[42] J.B. Buse, A. Garber, J. Rosenstock, W.E. Schmidt, J.H. Brett, N. Videbæk, J. Holst, M. Nauck, Liraglutide treatment is associated with a low frequency and magnitude of antibody formation with No apparent impact on glycemic response or increased frequency of adverse events: results from the liraglutide effect and action in diabetes (LEAD) trials, J. Clin. Endocrinol. Metab. 96 (2011) 1695–1702.
[43] I. Ozer, A. Tomak, H.M. Zareie, Y. Baran, V. Bulmus, Effect of molecular architecture on cell interactions and stealth properties of PEG, Biomacromolecules 18 (2017) 2699–2710.
[44] A.W. Richter, E. Akerblom, Antibodies against polyethylene glycol produced in animals by immunization with monomethoxy polyethylene glycol modified proteins, Int. Arch. Allergy Appl. Immunol. 70 (1983) 124–131.
[45] H.F. Stils Jr., Adjuvants and antibody production: dispelling the myths associated with freund's complete and other adjuvants, ILAR J. 46 (2005) 280–293.
[46] J.J.F. Verhoef, T.J. Anchordoquy, Questioning the use of PEGylation for drug delivery, Drug Deliv Transl Res 3 (2013) 499–503.
[47] A.M. Fathallah, R.B. Bankert, S.V. Balu-Iyer, Immunogenicity of subcutaneously administered therapeutic proteins—a mechanistic perspective, AAPS J. 15 (2013) 897–900.
[48] I.A. Ivens, W. Achanzar, A. Baumann, A. Brändli-Baiocco, J. Cavagnaro, M. Dempster, B.O. Depelchin, A.R. Rovira, L. Dill-Morton, J.H. Lane, B.M. Reipert, T. Salcedo, B. Schweighardt, L.S. Tsuruda, P.L. Turecek, J. Sims, PEGylated biopharmaceuticals: current experience and considerations for nonclinical development, Toxicol. Pathol. 43 (2015) 959–983.
[49] Y. Hou, S.A. Ernst, K. Heidenreich, J.A. Williams, Glucagon-like peptide-1 receptor is present in pancreatic acinar cells and regulates amylase secretion through cAMP, Am. J. Physiol. Gastrointest. Liver Physiol. 310 (2016) G26–G33.
[50] M. Bader, Y. Li, D. Lecca, V. Rubovitch, D. Tweedie, E. Glotfelty, L. Rachmany, H. K. Kim, H.I. Choi, B.J. Hoffer, C.G. Pick, N.H. Greig, D.S. Kim, Pharmacokinetics

and efficacy of PT302, a sustained-release Exenatide formulation, in a murine model of mild traumatic brain injury, Neurobiol. Dis. 124 (2019) 439–453.
[51] Z. He, Y. Hu, Z. Gui, Y. Zhou, T. Nie, J. Zhu, Z. Liu, K. Chen, L. Liu, K.W. Leong, P. Cao, Y. Chen, H.Q. Mao, Sustained release of exendin-4 from tannic acid/Fe (III) nanoparticles prolongs blood glycemic control in a mouse model of type II diabetes, J. Contr. Release 301 (2019) 119–128.
[52] K.V. Mann, P. Raskin, Exenatide extended-release: a once weekly treatment for patients with type 2 diabetes, Diabetes Metab Syndr Obes 7 (2014) 229–239.